Journal of Mineralogical and Petrological Sciences, Volume 115, page 118–137, 2020

REVIEW

The Indo-Eurasia convergent margin and earthquakes in and around Tibetan Plateau

Yanbin WANG[*], Yangfan DENG[**,***], Feng SHI[*,†] and Zhigang PENG[***]

[*]*Center for Advanced Radiation Sources, The University of Chicago, Chicago, IL, USA*
[**]*State Key Laboratory of Isotope Geochemistry, Guangzhou Institute of Geochemistry, Chinese Academy of Sciences, Guangzhou, 510640, China*
[***]*School of Earth and Atmospheric Sciences, Georgia Institute of Technology, Atlanta, GA, USA*
[†]*Present address: State Key Laboratory of Geological Processes and Mining Resources, China University of Geosciences, Wuhan, China*

After a brief review on tectonic settings of the Himalayas and Tibetan Plateau, we survey the literature on characteristics of earthquakes occurring in Tibetan Plateau and the surrounding regions. Shallow events (focal depths <50 km) show remarkable correlation with surface fault systems in both spatial locations and focal mechanisms. Some shallow events appear to be triggered by remote earthquakes and seasonal variations of ground water storage, suggesting stress levels nearing critical threshold. Intermediate-depth earthquakes (IDEQs; i.e., earthquakes with focal depths between 50 and 300 km) are concentrated beneath southern Tibet, the Hindu Kush-Pamir region, and the Burmese subductions zones. Underneath southern Tibet, the subducted Indian plate extends northward to at least the Bangong-Nujiang suture zone, with IDEQs occurring in the lower crust and the adjacent upper mantle. Possible mechanisms for IDEQs are also reviewed.

Keywords: Tibetan Plateau, Himalaya, Earthquake Triggering, Intermediate-Depth Earthquakes, Continental Collision Margins

AN OVERVIEW OF MAJOR GEOLOGICAL AND TECTONIC FEATURES OF TIBETAN PLATEAU

More than 200 million years ago (Ma), the Indian subcontinent (hereafter India) was a large island-like mass off the Australian coast and separated from Asia by the Tethys Ocean. After the breakup of Pangea around 200 Ma, India started drifting northward. Around 80 Ma, the Tethys Ocean floor was subducted under Asia. The thick sediments on the Indian margin of the ocean were scraped off and accreted onto the Eurasian continent, forming an accretionary wedge. Around 50 Ma, India's drifting rate slowed down significantly from about 15 to ~ 5 cm/yr (Avouac, 2015). In some models, this is interpreted as the beginning of the collision between Eurasian and Indian plates, the closing of the Tethys Ocean, and the initiation of Himalayan uplift. Other models suggest that the collision may have initiated earlier (Yin and Harrison, 2000).

doi:10.2465/jmps.190927
Y. Wang, wang@cars.uchicago.edu Corresponding author

Major surface features within Tibetan Plateau

Stretching over 2400 km from Pakistan to Burma, Himalaya is the most dominating topological feature on the surface of the Earth. The Himalayan thrust belt is an arc-like structure similar to island arcs in an oceanic subduction zone (Fig. 1a). This geometry may be inherited from the Indian-Tethys Ocean subduction prior to the continental-continental collision. The Himalayan Range can be divided into five sub-tectonic units from south to north (Fig. 1b): (1) The Sub-Himalaya, the foothill of the Himalayan range and composing primarily of Miocene-Pleistocene molassic sediments, is bounded in the south by the Main Frontal Thrust (MFT), which demarcates the principal displacement zone between the stable Indian continent and the Himalaya. (2) The Lesser Himalaya, which is mainly Upper Proterozoic-Lower Cambrian detrital sediments from the passive Indian margin, intercalated with some granites and volcanic rocks. These sediments are thrust over Sub-Himalaya along the Main Boundary Thrust (MBT). (3) The High Himalaya, which

is the backbone of the Himalayan orogen. Immediately north of MBT exposes a long band of metamorphic and igneous rocks known as the High Himalayan Crystalline Series, believed to be extruded mid- or lower-crustal materials (Harris, 2007). The High Himalayan Crystalline Series forms a major nappe which is thrust over Lesser Himalaya along the Main Central Thrust (MCT). (4) The Tethys Himalaya is a synclinorium formed by strongly folded and imbricated metamorphosed sedimentary series north of the MCT. In many places along the Himalayan belt, the transition from the low-grade sediments in Tethys Himalaya to low- to high-grade rocks of High Himalaya is marked by a major structure known as the South Tibetan Detachment System (STDS). (5) The Indus-Yarlun-Tsangpo Suture (IYS) zone, which represents the northern limit of the Himalaya and defines the zone of collision between the Indian plate and the Karakoram-Lhasa Block.

At least 1400 km north-south shortening has been estimated to be absorbed since the onset of the collision (Yin and Harrison, 2000). Figure 1b is a simplified tectonic map of the region. Tibetan Plateau is the largest area of high elevation and the thickest crust anywhere in the world, with an average elevation about 5000 m. It is bounded by the Altyn Tagh range and Kunlun and Qilian mountains in the north, the Karakorum and Pamir ranges in the west, and the Longmenshan range in the east. All of these boundaries are marked by major fault systems. Except for the giant thrust fault system in the south, almost all other boundaries are predominantly strike-slip in nature. Karakorum Fault (KKF; right-slip), Altyn Tagh Fault (ATF; left-slip), Haiyuan Fault (HYF; left-slip), and Xianshuihe-Xiaojiang Fault (XXF; left-slip) respectively mark the west, north, northeast, and southeast boundaries of the plateau. The northern segment of the eastern boundary separating Tibet from Sichuan Basin, also known as Longmenshan Thrust (LMT), is a series of west-dipping thrust fault systems.

Based on deformation features, Tibetan Plateau is commonly divided into three major segments separated by sub-parallel suture zones that are more than 1000 km in length running roughly east-west (Fig. 1). Southern Tibet (Lhasa Terrane) lies between IYS and Bangong Nujiang Suture (BNS) zones, central Tibet (Qiangtang Terrane) lies between BNS and Jinsha suture (JS) zones, and northern Tibet (Songpan-Ganzi Terrane) between JS and Anymaqen-Kunlun-Muztagh Suture (AMS) zone, the last of which borders Tarim and Qaidam Basins. In central Tibet, another suture, Longmu Co - Shuanghu Suture (LSS), divides Qiangtang Terrane into south and north Qiangtang (Fig. 1b). North of AMS and east of ATF is Kunlun-Qaidam terrane. Receiver function studies show that most of the large suture zones are subvertical shear zones which may extend to ~ 100 km depth in the upper mantle (Zhang et al., 2014). Whether the entire plateau was lifted more-or-less uniformly over time is still debated. A recent discovery of fossil palm leaves from the sediment of Lunpola Basin (near BNS), dated about 25 Ma, suggests that the floor of the basin was no higher than 2.3 km at the time. This, in turn, suggests that a paleo-valley existed in present-day Lhasa Block, bounded by ~ 4 km high mountains (Su et al., 2019).

Numerous fault zones in Tibet have been reviewed by Taylor and Yin (2009) and Yin et al. (1999). Major faults are running approximately east-west, subparallel to the major suture zones and normal to the Indian plate motion. These include, from south to north, MFT, MBT, MCT, STDS, Shiquanhe-Ganze-Amdo (SGA) thrust system, the Great Counter Thrust (GCT), and Gangdese Thrust (GT). Additional details can be found in Taylor and Yin (2009). Most are thrust faults in nature, except for STDS and GCT, which are normal faults. Kunlun Fault (KLF), near the northern end of Tibetan Plateau, is a left-slip strike-slip fault (Taylor and Yin, 2009).

Global positioning system (GPS) velocities show that present-day surface strain field of western Tibet (west of ~ 85°E) is dominated by northward shortening, with north-ward GPS velocities decreasing monotonically from 4 cm/yr at the southern edge of the Himalaya to less than 0.5 cm/yr at the Tarim Basin boundary (Zhang et al., 2004b; Gan et al., 2007). Especially near Pamir and Hindu Kush, east-west velocity components are negligibly small. East of 85°E, GPS velocities rotate gradually from north-ward to east-ward. Component of east-ward velocity increases from near 0 cm/yr at the west end of Tibetan plateau to a maximum of 2.5 cm/year around 95°E and then decreases to less than 0.5 cm/yr near LMT (Zhang et al., 2004b; Gan et al., 2007). North of the Indo-Burmese subduction zone, GPS velocities turn sharply from SW-NE to NW-SE. The strain fields inferred from these velocity directions are generally consistent with an extruded Tibetan crust towards South China.

Another important deformation feature within Tibetan Plateau is the active rift systems, which are mostly located between the suture zones (Fig. 1a). Within southern Tibet (south of BNS), there are at least seven prominent rift systems, starting from Nari Yun Chu (~ 92°E) westward: Yadong-Gulu (~ 90°E), Pumqu-Xianza (88°E), Tangra Yum Co (86°E), Xiakangjian (85°E), Lunggar (83°E), and Yari (82°E). These rifts are normal fault systems approximately parallel to the direction of India-Asia relative motion and perpendicular to the suture zones. Between BNS and JS (central Tibet), there are 9 large rift systems, which tend to fan out and are roughly

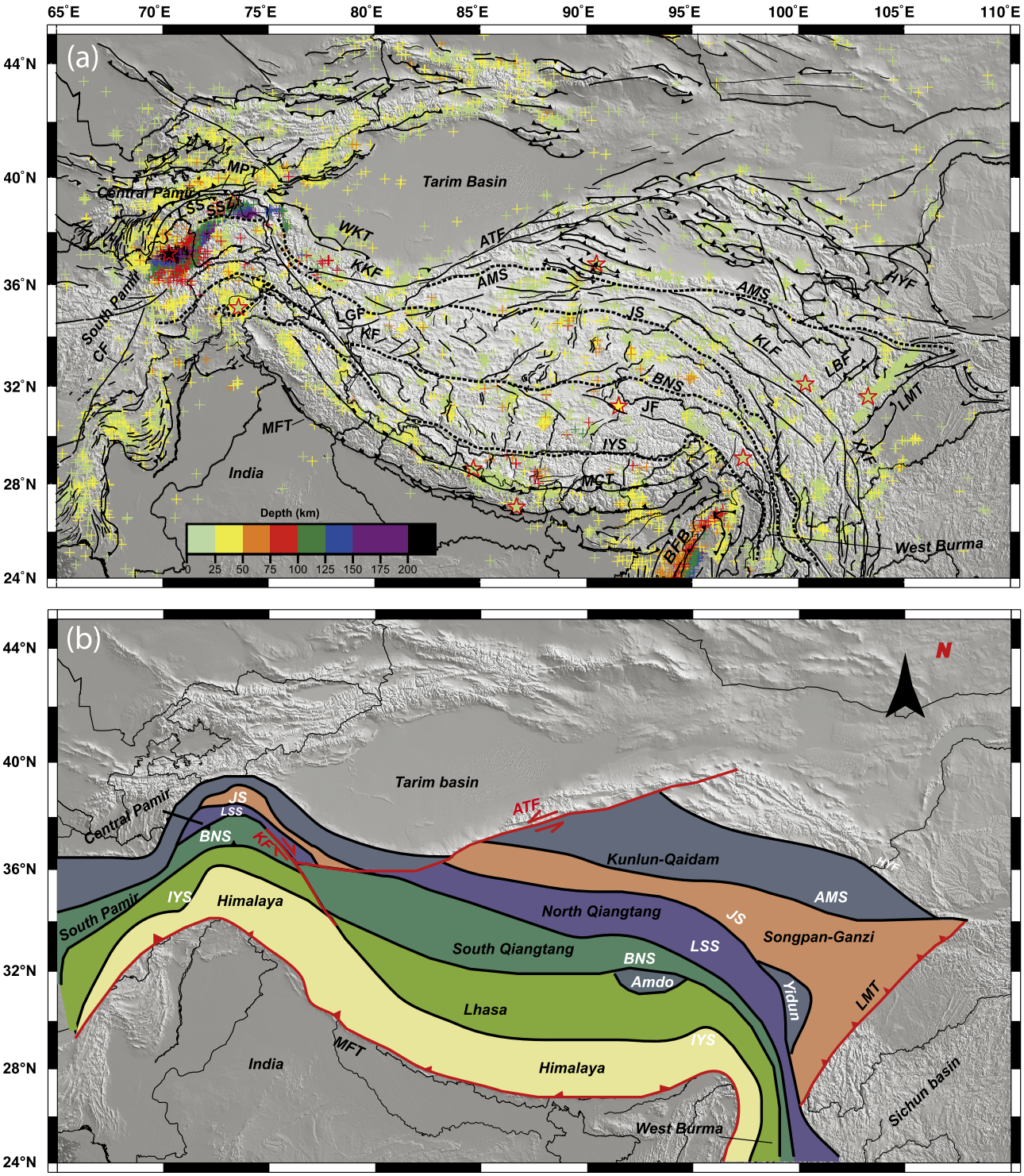

Figure 1. (a) Map of Tibetan Plateau and surroundings, showing earthquake epicenters (+, event depths are color coded). The Himalaya thrust belt consists of three thrust systems (from south to north): main boundary thrust (MBT), main frontal thrust (MFT), and main central thrust (MCT). Only MFT and MCT are shown. Large historic events (M > 7.5) are shown as stars. Major fault systems and suture zones are also marked. Major suture zones: AMS, Anymaqen-Kunlun-Muztagh suture; BNS, Bangong Nujiang suture: IYS, Indus Yalu suture; JS, Jinsha suture; LSS, Longmu Co-Shunghu suture; SSZ, Shyok suture zone. Major left-slip faults: ATF, Altyn Tagh fault; KLF, Kunlun fault; CF, Chaman fault; HYF, Haiyuan fault; XXF, Xiangshuihe-Xiaojiang fault system; KKF, Karakash fault; LGF, Longmu-Gozha fault. Major right-slip faults: KF, Karakoram fault; JF, Jiali fault; LBF, Longriba fault. Major fold-thrust belts: WKT, Western Kunlun Thrust; LMT, Longmenshan Thrust; BFB, Burmese fold belt, MP, Main Pamir Fault. (b) Simplified major tectonic terrains of Tibet and surroundings.

within ±45° from the direction of Indian plate subduction.

Two sets of smaller-scale strike-slip fault systems are distributed nearly symmetrically relative to BNS, forming a series of V-shaped conjugate faults in central Tibet, with the sharp end of the 'V' pointing to the west. Both fault systems are 25-35° away from BNS. While the faults north of BNS are left-slip, those south of BNS are right-slip. Yin and Taylor (2011) attribute this conjugate fault complex to a mechanically weaker central Tibet between more rigid southern and northern Tibet. As the subducting Indian plate plows northward compressing the entire Tibetan Plateau along the N-S direction, central Tibet flows eastward, as indicated by the GPS velocity field (Gan et al., 2007), resulting in two east-trending shear zones: a northern left-slip zone consisting of active left-slip faults just south of JS, and a southern right-slip zone consisting of active right-slip faults north of IYS. The central Tibet conjugate faults may have initiated as two sets of Riedel shears in the two parallel but separate shear zones. A recent upper crustal model of central Tibet based on velocity and attenuation tomography supports this model (Zhou et al., 2019).

Major features of surrounding regions

South of 27°N and east of 96°E, in the Indo-Burma ranges and subduction zone, Indian plate plunges eastwards under the Burmese arc (Khan, 2005; Angelier and Baruah, 2009). Near 28°N and 96°E, eastern Himalayan mountains meet Indo-Burma ranges, the western edge of Burma plate (Fig. 1). In this region, the Assam syntaxis zone is bounded by the MBT units of the easternmost Himalayas to the north and the northernmost Burmese arc to the south. Both thrust systems run parallel, trending ENE-WSW. The complicated converging structures severely deform the northeastern portion of the India plate (Chen and Molnar, 1990; Bilham and England, 2001), although the deformation state is poorly understood.

The northwestern end of Himalayan syntaxis and Karakorum ranges merge to connect with the Hindu-Kush range in northern Afghanistan (Fig. 1). Further north of Hindi-Kush is the Pamir mountain, which neighbors with Karakorum ranges in the south and Kunlun ranges in the east. The Sarez-Murghab Thrust System (SMTS) in Pamir dips towards Hindu-Kush and Himalayas, with increasingly deeper seismicity to southeast, interpreted as another intercontinental subduction zone (Schurr et al., 2014). The Pamir and Hindu Kush regions are unique in featuring intense Intermediate-depth earthquakes (IDEQs) to almost 300 km depth in an intracontinental setting (Zhan and Kanamori, 2016; Kufner et al., 2017; Li et al., 2018a), testifying to vigorous geodynamic processes in the mantle below.

In the southwest, MFT turns sharply from W-E to NE-SW near 70°E (northern Pakistan), cutting through western Pakistan and eastern Afghanistan (Fig. 1), where the northward collision in the Himalayas translates into dip-slip faults. The most significant among them is the Chaman Fault (CF), which is a primarily transform, left-lateral strike-slip fault, responsible for numerous major earthquakes in Pakistan and Afghanistan (Mahmood et al., 2015).

Deep structures of Tibet and surrounding regions

Seismic surveys of the Tibetan Plateau began in 1958, first by Chinese scientists (Zeng et al., 1961) and then by international teams. International seismic campaigns such as INDEPTH (International Deep Profiling of Tibet and the Himalaya) (Zhao et al., 1993; Nelson et al., 1996), Hi-CLIMB (Himalayan-Tibetan Continental Lithosphere During Mountain Building) (Nábělek et al., 2009), and HIMNT (the Himalayan Nepal Tibet Seismic Experiment) (Sheehan et al., 2008) have accumulated large amounts of broadband seismic data.

Based on these data, Mechie et al. (2011) constructed an average seismic velocity model of Tibet Plateau to 700 km depth. Zhang et al. (2011) summarized 35 years of deep seismic sounding studies and concluded that crustal thickness is ~ 70-75 km under southern Tibet and 60-65 km under northern, northeastern and southeastern Tibet. This is consistent with a recent model of the crust-mantle boundary (Mohorovičić discontinuity, or Moho) in the region (Baranov et al., 2018) (Fig. 2). The Moho model is based on combined seismic and gravity data and reflects large length scale depth variation. At shorter scales, Moho depth exhibits significant variations, especially in southern Tibet, partly influenced by the deep-rooted rift systems, making local Moho depth determination difficult (Li et al., 2011). Various analyses, based on gravity (Hetényi et al., 2007; Jiménez-Munt et al., 2008), body wave tomography (Tilmann and Ni, 2003; Zhou and Murphy, 2005; Liang et al., 2016), Rayleigh wave tomography (Ceylan et al., 2012), Pn velocity tomography (McNamara et al., 1997; Liang and Song, 2006; Li and Song, 2018), multiple wave adjoint tomography (Chen et al., 2017), shear wave splitting (Huang et al., 2000; Chen et al., 2010), and receiver functions (Kind et al., 2002; Zhao et al., 2010; Zhao et al., 2011, etc.) show consistently that Tibet is underlain by a relatively cold, high velocity anomaly that are about 150 km thick. This anomaly is generally interpreted as the more rigid Indian continental lithosphere, whose leading edge reaches various latitudes under west, central and east Tibet.

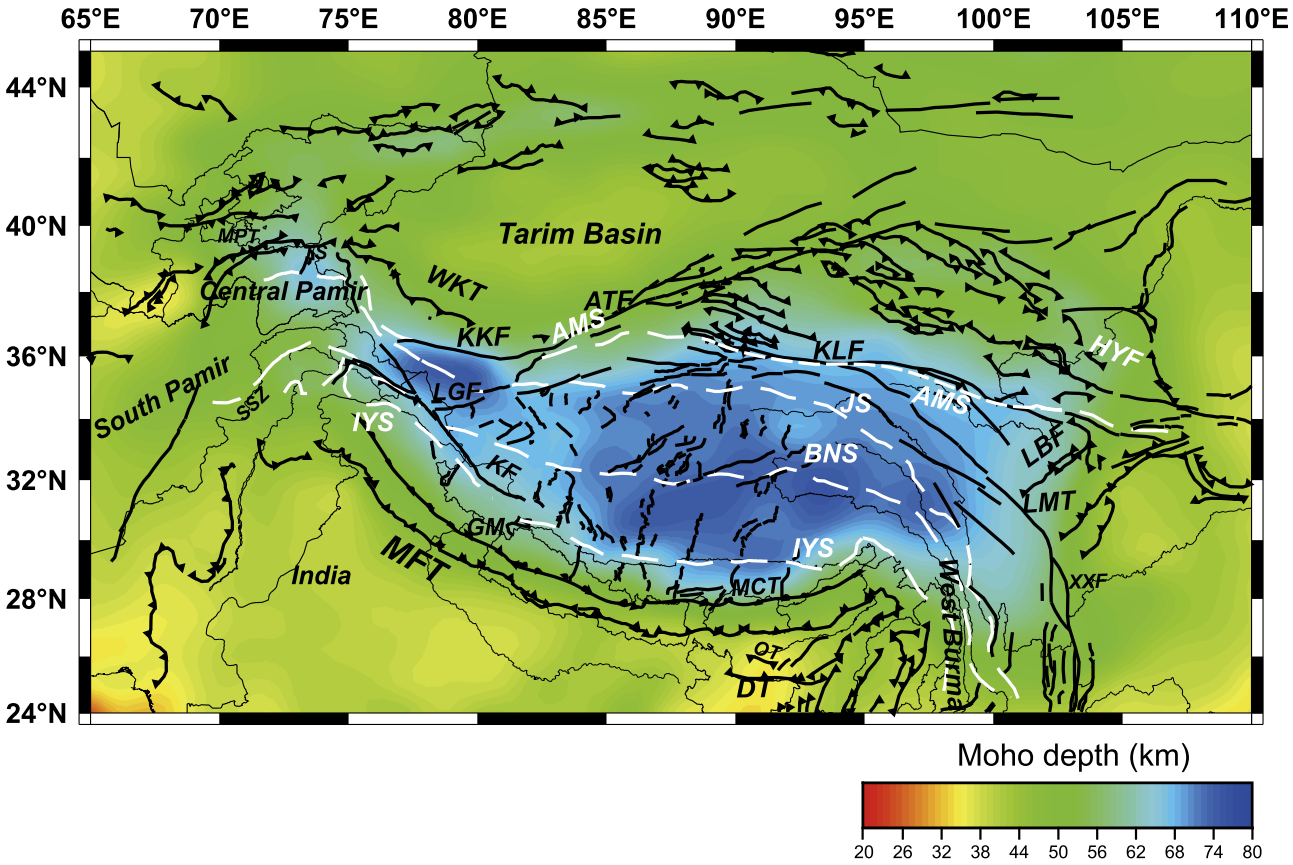

Figure 2. Moho depth contours under southern Tibet, based on combined gravity and seismological data based on the results from (Baranov et al., 2018).

Wide-angle seismic data show that the Moho has two separate depressions, one runs SE-NW from (~ 29°N, 90°E) to (36°N, 80°E) reaching the southern boundary of Tarim Basin, the other is centered around BNS (30-34°N) between 90 and 95°E (Zhang et al., 2011). These are interpreted as signatures of subducted Indian plate, which is torn apart. These observations are in general agreement with results from P-wave tomography imaging (Kumar et al., 2006; Li et al., 2008; Nábělek et al., 2009; Kind and Yuan, 2010; Zhao et al., 2010). While Li and Song (2018) suggested that beneath eastern Tibet the Indian plate may reach beyond JS, Zhou and Murphy (2005) argued that the Indian plate may underthrust across the entire plateau.

Recent studies reveal an aseismic layer in the mid-crust under Tibetan Plateau (Sloan et al., 2011; Shen et al., 2016). Hetényi et al. (2011) studied the crustal structure of southern Tibet and found patchy presence of low-velocity layers (LVLs), which appear to be correlated with the rift systems, with vertical extension of ~ 10 km and maximum horizonal length on the order of 50 km only. They concluded that partial melt is not widespread in southern Tibetan crust and questioned the model of channel flow (e.g., Royden, 1996, also see Grujic, 2006 for a review) to accommodate the ongoing convergence between the Indian and Eurasian plates. Using Rayleigh-wave tomography, Jiang et al. (2011) observed a LVL in the middle crust beneath Lhasa Terrane, prominent low-velocity anomalies from the lower crust to the mantle lithosphere along the N-S trending Tangra Yum Co rift and the Pumqu Xianza rift, and a slab-like high velocity anomaly beneath both the Himalayas and the Lhasa Block. They suggested that central southern Tibet is currently underlain by segmented Indian lower crust and mantle lithosphere. Similarly, Chen et al. (2015) proposed slab tearing under several rifts (Xainza-Dingjye Nyima-Tingri, and Longgar) in central Tibet, according to SKS-wave splitting measurements. This is broadly consistent with the high-resolution P and S wave tomography model of Li and Song (2018), which showed that the subducted Indian mantle lithosphere is torn into at least four pieces with different dipping angles and northward limits, shallower and extending further in the west and east ends while steeper in between. The latter study

also found that intermediate-depth earthquakes (IDEQs), i.e., event with focal depths between 50 and 300 km, in the lower crust and mantle are located almost exclusively in the high-velocity (and presumably strong) parts of the Indian lithosphere.

Northeastern Tibet is characterized by blocks of NW-SE extending mountain terrains, including Songpan-Ganzi, Kunlun-Qaidam, Central Qilian, and Northern Qilian mountains, which deform continuously but are separated by several major active thrusts and sinistral strike-slip faults such as KLF, south Qilian suture, HYF, and Gulang Fault. Deng et al. (2018) reported a major LVL beneath Songpan-Ganzi terrain at ~ 30 km depths. It penetrates the KLF, continues towards shallower depths, and then abruptly dips to below 40 km beneath central Kunlun-Qaidam terrain. Further NE, the LVL becomes more segmented with a number of abrupt jumps, generally towards shallower depths, before completely vanishing beneath North China Craton. A major Moho offset on the order of 20 km is observed directly beneath the HYF, suggesting that this fault extends deep into the upper mantle. In fact, Moho offsets are associated with essentially all major fault systems in this area (Vergne et al., 2002; Ye et al., 2015; Liu et al., 2017), reaching as deep as ~ 60 km. Overall, these observations suggested that the growth of northeastern Tibet plateau is characterized by lithospheric-scale staged deformation of continuous shortening.

The cause of the rift systems in Tibetan Plateau is still debated. Mean spacing between rifts decreases systematically from south to north (Yin, 2000). The widely spaced rifts in the Himalaya and southern Tibet are interpreted as the result of a relatively light crust atop a strong Indian mantle lithosphere, whereas the systematic decrease in rift spacing northward is due to decreasing crustal thickness from south to north (Yin, 2000). The E-W extension of the rift systems is attributed to the brittle Indian mantle lithosphere underneath Tibet: rifts initiate from subducted Indian mantle lithosphere, which is thinned in response to extension by both brittle faulting from within and by ductile flow from below due to asthenospheric upwelling. These lithospheric faulting events are considered responsible for the rifts and syn-rifting magmatism (Yin, 2000). Such interpretation is consistent with the aforementioned seismic imaging results. An alternative view is that the rifts are predominantly an elastic response of the brittle Tibetan crust to the indentation of the Indian plate (Kapp and Guynn, 2004). In this view, the rift systems are interpreted as high shear and differential stress regions due to the northward insertion of the Indian plate (Kapp and Guynn, 2004), causing Tibetan Plateau to shorten in S-N direction and extrude E-W.

Thermal structure

Thermal structure is crucial in understanding the origin of seismic activities in Tibet but remains poorly understood. Heat flow data show relatively high mean values, ~ 75 mW m^{-2} in central and southern Tibet, with an anomaly as high as ~ 150 mW m^{-2} centered around Lhasa (Tao and Shen, 2008). Constrained by these data, Zhang et al. (2013) showed that geotherms are higher in the south and become colder northward. Searle et al. (2006) gave a geotherm model for southern Tibet where the upper crust is significantly hotter than the lower crust. Such a temperature inversion appears consistent with widespread LVLs in the upper/mid crust (Shen et al., 2016). Mafic xenoliths from central Tibet record a steep thermal gradient reaching ~ 800-1000 °C at depths of 30-50 km (Hacker et al., 2000), broadly consistent with the calculations by Zhang et al. (2013). P-wave velocities and Poisson's ratios extracted from seismic observations, as well as the lack of hydrous minerals, suggest that crustal melting under Tibet was not widespread (Hacker et al., 2000). Numerical simulations based on field observations and rock physical properties (Wang et al., 2013) indicated that although the entire collision system is cooled by the northward-advancing Indian lithosphere beneath Tibet, the upper and middle crust may be warmed by shear heating, which explains the mantle xenolith data (Hacker et al., 2000), supporting a warm upper crust over a cold upper mantle. The temperatures inferred from a combination of numerical simulation and mineral physics suggest that lower crust and the upper mantle beneath central Tibet are weak and prone to flow toward adjacent areas (Deng and Tesauro, 2016). The subducted Indian plate is a distinct low-temperature feature beneath South Tibet.

Thermal state of the subducted Indian plate has been investigated by thermokinematic modeling combined with experimentally derived flow laws. The cold Indian lithosphere slowly warms as it subducts northward. Modeling showed that ~ 400 km north of the Himalaya Front, cold core of the Indian plate may reach ~ 600 °C (Craig et al., 2012). If the Indian lower crust is anhydrous, it will remain strong beneath the southern half of the Tibetan plateau. In northwest Tibet, the strong underthrust Indian lower crust abuts the rigid Tarim Basin and may be responsible for both the clockwise rotation of Tarim relative to stable Eurasia and the gradient of shortening along the Tien Shan. Receiver functions studies support this inference of temperature, and further suggest that eclogitization of granulite-facies rocks in Indian plate may begin around this temperature (Schulte-Pelkum et al., 2005).

SEISMICITY IN AND AROUND TIBETAN PLATEAU

Our search through the International Seismological Center (ISC) database with hypocenter depth corrected based on the EHB algorithm (Engdahl et al., 1998) yielded ~ 7200 earthquakes over the region 24°N–40°N and 65°E–105°E in a period of 43 years (1972–2015). Epicenters of these events are over-plotted in Figure 1a, with focal depths color-coded. A high concentration, nearly continuous belt of earthquakes is along MCT, with focal depths restricted to within 50 km from the surface. North of MCT, deeper events up to 100 km are mostly between 80 and 95°E, with higher concentration beneath southern Tibet. Around the junction of India–Tibet–Burma (also known as the Eastern Syntax) and in Pamir – Hindu Kush region, events deeper than 200 km are highly concentrated. Historic large earthquakes with magnitude greater than 7.5, also shown in Figure 1a, are mostly located in the three aforementioned regions, as well as along the eastern boundary of Tibetan Plateau (e.g., near the LMT and XXF). The 1950 Assam–Tibet earthquake (M_w 8.6) is the largest earthquake ever recorded outside oceanic–continental subduction zones. Other well-known examples include the 2008 Wenchuan earthquake (M_w 7.9), the 2015 Nepal earthquake (M_w 7.8), and the 2015 Hindu Kush earthquake (M_w 7.5), all of which caused significant live loss and property damage.

In order to examine earthquake distribution to more details, we divided the entire area (Fig. 1) into 8 slices with 2° latitude from 24 to 40°N and plotted event depth versus longitude (Fig. 3). Between 24 and 26°N latitude, deep events are concentrated within the Indo–Burmese subduction zone (92–98°E). Elsewhere, no events are below 50 km depth. Between 26 and 28°N, another column of deep events to ~ 100 km depth is within southern Tibet (85–90°E). Between 28 and 30°N, deep events are more spread-out in longitude (~ 85–95°E) in southern Tibet. Similar deep event distribution continues in the slices 30–32°N to 34–36°N, with decreasing maximum depth and event density. Deep events in the slice 34–36°N are dominated by those in Hindu Kush and Pamir (70–80°E). In slices 36–38°E and 38–40°E, all events deeper than 50 km are in Hindu Kush and Pamir and depths of ~ 300 km.

We also divided the area (Fig. 1) into 8 slices with 5° longitude from 65 to 105°E and plotted event depth versus latitude (Fig. 3). For the slices up to 80°E, all events deeper than 50 km are in Hindu Kush and Pamir (36–40°N). Within Tibetan Plateau, no events are deeper than 50 km between 80 and 85°E. Between 85 and 90°E, a large number of events occurred in southern Tibet (27–36°N), with decreasing event density northward. Between 90 and 95°E, dominant deep events are in the Indo–Burmese subduction zone (south of 27°N).

The above examination shows that within Tibet, events are predominantly shallow, generally within the top 50 km depths. Events with M > 6 are essentially all within the top 30 km depths, where event clusters show remarkable spatial correlation with surface features (Fig. 1). IDEQs beneath Tibetan Plateau appear to concentrate in southern Tibet exclusively and their depths reach >100 km continuously (Fig. 3). This observation, however, is debated. Some authors reported absence or decreasing activity of IDEQs within the lower crust (e.g., Chen and Molnar, 1983; Zhu and Helmberger, 1996; Monsalve et al., 2006; Liang et al., 2008; Schulte-Pelkum et al., 2019). The tectonic implication is that the lower crust is either too strong to fail under the tectonic stresses (Watts and Burov, 2003) or too soft to be seismogenic (Chen and Molnar, 1983). Others found sufficiently high seismicity within the lower crust under southern Tibet (e.g., Maggi et al., 2000; Jackson, 2002; Priestley et al., 2008).

Whether IDEQs are located dominantly in the upper mantle or in the subducted Indian plate depends critically on the determination of Moho depth. Earlier locations of events below the Moho (Chen and Molnar, 1983) were later corrected to be above the Moho (Maggi et al., 2000; Jackson, 2002). On the other hand, Schulte-Pelkum et al. (2019) corrected data reported by Monsalve et al. (2006) and concluded that majority of the events were located in the upper mantle. It is now well-known that velocity structure under southern Tibet has significant lateral variations (e.g., Li and Song, 2018). Treating steeply varying Moho as a flat, one-dimensional discontinuity may result in large uncertainties and artifacts (Li et al., 2011). Several lines of evidence suggest that at least some of the IDEQs are originated within the lower crust: (1) IDEQs are restricted to southern Tibet, whereas the shallow strike-slip and normal faulting are widespread. (2) Locations of the IDEQs are closely related to expected locations of subducted Indian plate under southern Tibet; e.g., some IDEQs (e.g., Monsalve et al., 2006) correlate with segmented high velocity anomalies from seismic tomography imaging, used as evidence of break-up of the Indian plate (e.g., Li and Song, 2018). (3) Where IDEQs are observed, gravity anomalies and flexure analyses yield an effective elastic thickness of the lithosphere as thick as 100 km (Jordan and Watts, 2005), suggesting continued rigidity of the lithosphere. (4) Numerical modeling (Copley et al., 2011) shows that the predominantly normal faulting focal mechanisms within southern Tibet and strike-slip faulting in northern Tibet are a result of strong mechanical coupling between

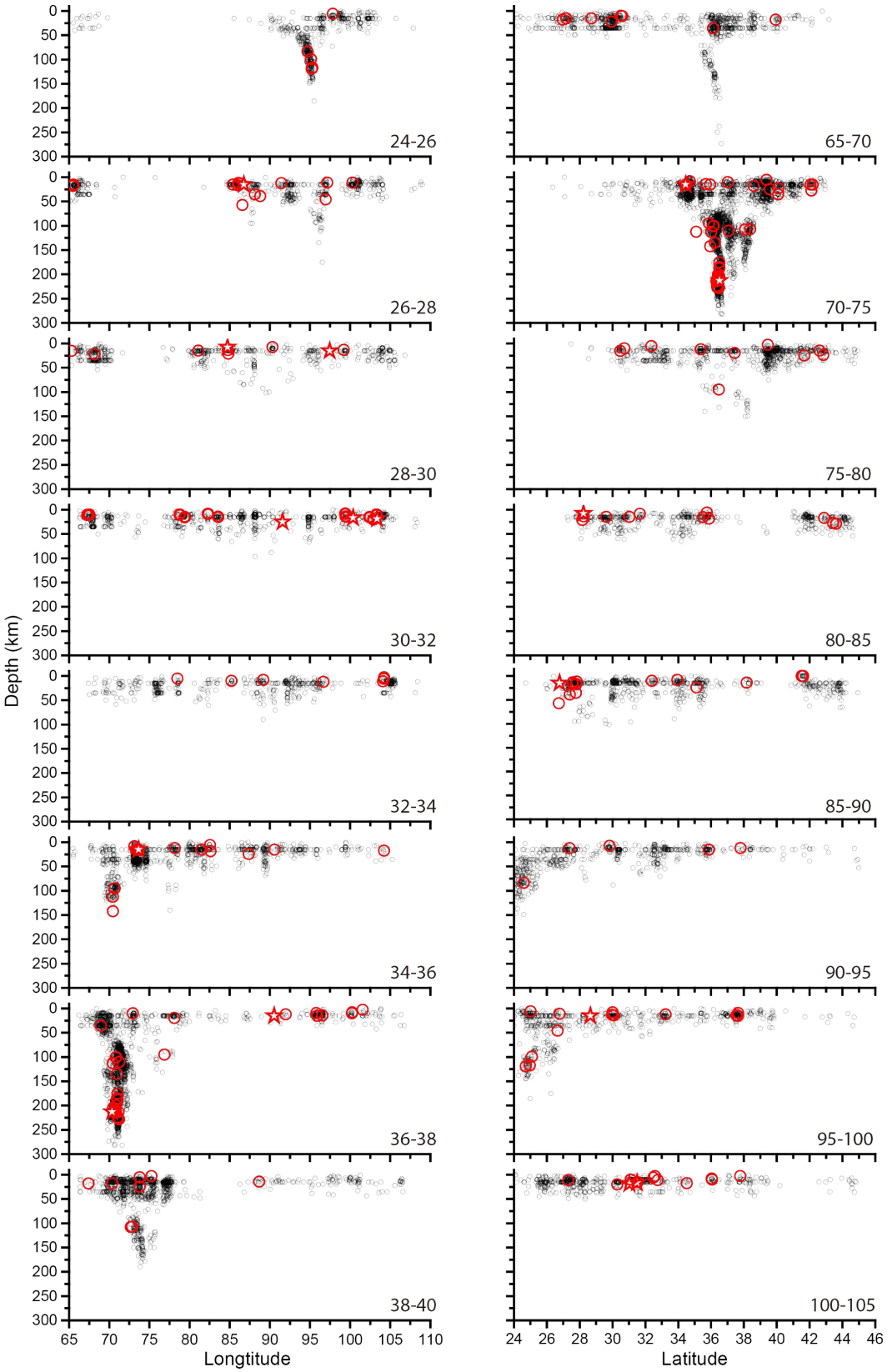

Figure 3. Distribution of earthquakes in and surround Tibetan plateau. Left column: Event depth distribution versus longitude in 2° slices of latitude from 24 to 40°N. Right column: Event depth distribution versus latitude in 5° slices of longitude from 65 to 105°E. Events with M > 6 are plotted as red circles and those with M < 6 are black circles. Red starts are the historically large events plotted in Figure 1.

the subducting Indian plate and the overriding plateau in southern Tibet. This implies a strong Indian plate above the Moho. Furthermore, if the lower crust is the weakest layer with negligible coupling to the upper mantle, one needs additional driving forces for the IDEQs immediately below it.

Earthquake focal mechanisms within Tibetan plateau – shallow events

Many authors have examined earthquake focal mechanisms in Himalaya and Tibetan plateau with event magnitude >5 (e.g., Chen and Molnar, 1983; Molnar and Lyon-Caen, 1989; Zeng and Sun, 1993; Copley et al., 2011) and showed that for shallow earthquakes, focal mechanisms generally are reasonably well divided into southern and northern regions, with their boundary roughly corresponding to the leading edge of subducted Indian plate (Fig. 4a). While earthquakes in northern Tibet are dominated by strike-slip mechanisms, those in southern Tibet are primarily normal faulting. There are essentially no earthquakes deeper than 50 km in northern Tibet, whereas in southern Tibet earthquakes as deep as 100 km are not uncommon. This is consistent with the estimated seismogenic thickness (Ts) being rather flat for central and northeastern Tibet but highly variable along the strike of the Himalayan foreland (Bai et al., 2017).

South of the plateau, along the Himalaya mountain range, focal mechanisms indicate predominantly north-dipping thrust faulting (Fig. 4a). The dominance of thrust faulting mechanisms continues westward along the Himalaya, reaching Nanga Parbat (72°E, 35°N). From there and further north to Pamir and Hindu Kush, focal mechanisms of normal, thrust, strike-slip characteristics can all be found. In the northern boundary and west of central Tarim Basin, focal mechanisms are also complex. The east portion near Burma, on the other hand, is generally characterized by left-lateral strike-slip focal mechanisms (Fig. 4b).

In eastern Tibet (Fig. 4c), along the northern segment of the boundary (i.e., LMT), earthquakes are largely west-dipping thrust faulting, whereas the southern segments (XXF and JF) are dominated by right-lateral strike-slip. Cui et al. (2019) analyzed focal mechanisms of 725 earthquakes between 1976 and 2017 in the North-South Seismic Belt (NSSB; 21°N-42°N, 97°E-107°E). They found that the ***P***-axes of focal mechanisms rotate clockwise, from SW-NE trending in the north, to W-E in the middle, and NW-SE or even N-S in the south of the NSSB. This pattern is generally consistent with the GPS velocity fields relative to the stable Eurasia (Gan et al., 2007), with thrust-dominated focal mechanisms along the LMT, and strike-slip near the south end of the XXF and JF.

Focal mechanisms within Tibetan Plateau – IDEQs

For a dozen IDEQs in southern Tibet (28-30°N, 83-90°E) with focal depths below 60 km, De La Torre et al. (2007) showed that, from the Himalaya to southern Tibetan, strike-slip faulting is dominated by ***P***-axes trending NNW-SSE to NNE-SSW and shallow plunging ***T***-axes. They concluded that strike-slip faulting and EW extension accommodate the deformation near and below the Moho. The strike-slip clusters beneath the High Himalaya contains two groups: one about 200-300 km north of the Himalayan arc with depths from 80-100 km, and the other around 28°N with depths ranging from 60-100 km. Strike-slip faulting dominates both groups with only one exception which is normal faulting. They concluded that IDEQs near the Moho under the High Himalaya are common. In contrast, Chen and Yang (2004) argued that earthquakes at this depth range are unrelated to subduction processes due to faulting similarities to the upper Tibetan crustal focal mechanisms and faulting differences to earthquakes along the Himalayan front. De La Torre et al. (2007) pointed out that fault plane solutions for the events at depths >60 km have horizontal ***P***-axes nearly parallel to the convergence direction and parallel to the ***P***-axis orientations of shallow thrust earthquakes. They argued that these ***P***-axis orientations suggest a correlation between the convergent process and the earthquakes at Moho depths.

Earthquake focal mechanisms in Assam-Tibet area

In southeast Tibet, three major tectonic units interact along two convergent boundaries: the Himalayas, Bengal Basin, and the Indo-Burma Ranges. All three units meet at the Assam Syntaxis. This region has been the site of some of the largest continental earthquakes (Assam, 1950, moment magnitude M_w = 8.6; Shillong, 1897, $M_w \approx 8.1$) (Angelier and Baruah, 2009).

From spatial distribution and focal mechanisms reported by Kumar et al. (2015) and the GCMT catalog (Ekström et al., 2012), this region may be divided into four sub-domains (Fig. 4b). The N-S convergence is accommodated through shallow thrust earthquakes within the Himalayan wedge (region 1). Strike-slip earthquakes are distributed in the region sandwiched between Himalaya and Indo-Burma Ranges (region 2), where widespread N-S compression in Shillong Plateau, far away from the Himalayan front, is compatible with previously proposed convergence between the Shillong-Mikir-As-

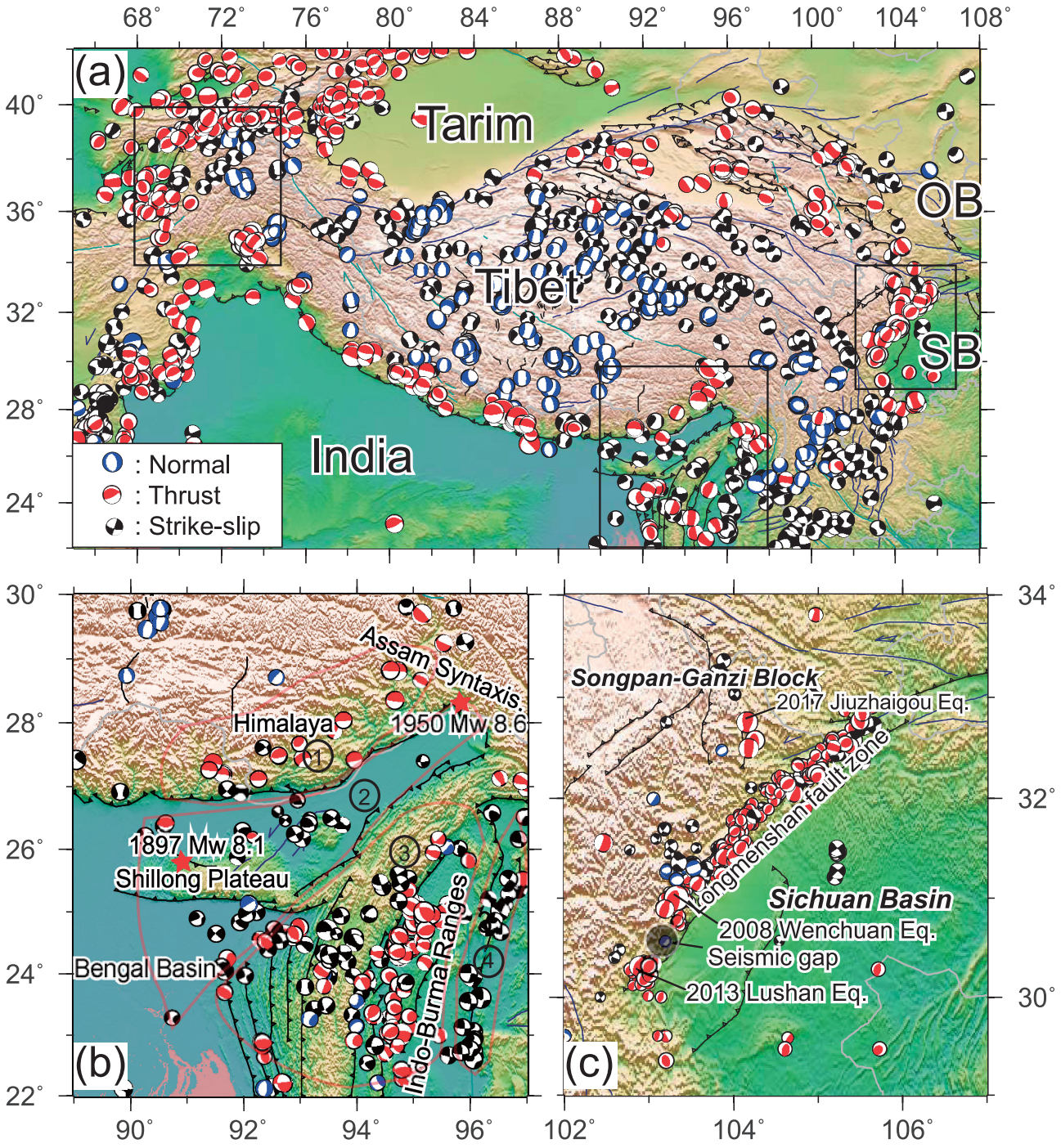

Figure 4. (a) Focal mechanisms of shallow earthquakes (<50 km) for the entire Tibetan Plateau (GCMT catalog). Beachball solutions are color-coded for thrust (red), normal (blue), strike-slip (black) events. Tibetan plateau is surrounded by thrust faulting events around its southern boundaries. Normal faulting events are primarily associated with rift systems in southern Tibet, whereas strike-slip events are concentrated around JS and northern Tibet, where thrust faulting events are also common. (b) Focal mechanisms in Assam-Tibet (GCMT catalog and Kumar et al., 2015). The four subdomains are outlined, classified according to focal mechanisms. See details in text. (c) Focal mechanisms at and near LMT (GCMT catalog and Li et al., 2019b). The approximate rupture areas of the 2008 Wenchuan and 2013 Lushan earthquakes are marked by gray line. The gray circle marks the inferred seismic gap between the Wenchuan and Lushan earthquake ruptures.

sam Valley block and the Indian craton (Angelier and Baruah, 2009). The E-W subduction results in earthquakes whose mechanisms vary from thrust faulting at shallow depths to strike-slip at intermediate depths, and then to thrust faulting again underneath the Indo-Burma convergence zone (region 3) (Kumar et al., 2015). To the

east of Indo-Burma (region 4), earthquakes are dominated by dextral strike-slip stresses. Such stresses are accommodated by the extrusion of the Tibetan material from north to the south.

Earthquake focal mechanisms along Longmenshan Thrust Fault

The LMT and its surrounding regions have produced a number of devastating earthquakes. The 2008 M_w 7.9 Wenchuan, 2013 M_w 6.6 Lushan, and 2017 M_w 6.5 Jiuzhaigou earthquakes are just a few examples. While the first two exhibit clear thrust fault features along the convergence boundary, the third event occurred on the strike-slip fault system (i.e., the Huya fault) within Tibetan Plateau. Based on waveform inversion, Li et al. (2019b) reported focal mechanisms of earthquakes occurred between 2009 and 2016 in this region (Fig. 4c), showing a dominant thrust faulting stress regime with subhorizontal NW-SE trending maximum principal stress (σ_1) and subvertical minimum principal stress (σ_3). These observations indicate a lateral compression due to the southeast-ward movement of the Songpan-Ganzi Block. The observed changes in dip are used to infer a detachment layer in the upper crust. Based on the determined source parameters, Yang et al. (2017) concluded that the southern segment of the LMT is characterized by thrust faulting stress regime with a nearly horizontal σ_1 in the SE-NW direction, while the stress environment in the northern segment is much more complicated.

Only a few earthquakes occurred between the Wenchuan and Lushan rupture zones, suggesting a possible seismic gap (Fig. 4c). There are two contrasting views on this gap. Based on Pg tomography and the theory of maximum effective moment, Pei et al. (2014) argued that this region is weak and ductile in nature and cannot accumulate stress to generate large ($M > 7$) earthquakes. Liu et al. (2018) observed a LVL and a thick crust in this region; they associated the LVL with partial melt to account for the aseismic feature. Based on paleoseismic activity, Shao et al. (2019) also concluded that rocks in this gap are ductile with low strength, although they found four paleoseismic events. However, some authors argued that this may be a high-risk area for future large earthquakes (e.g., Gao et al., 2014).

Earthquake focal mechanisms in Hindu Kush area

Hindu Kush is one of the most seismically active areas in continental regions, famous for intense IDEQs (Prieto et al., 2012). Examples of large IDEQs in the Hindu Kush include the 9 August 1993 (M_w 7.0, depth 214 km), the 3 March 2002 (M_w 7.3, depth 229 km), and the 26 October 2015 (M_w 7.5, depth 209 km) earthquakes, all of which caused severe damages in Afghanistan and Pakistan (Rehman et al., 2015; Rehman et al., 2017).

Based on the GCMT catalogue (Ekström et al., 2012), most of the focal mechanisms in this region are compressional, and earthquake occurrence rate has a bimodal distribution in depth, with Groups I and II seismicity peaking around ~ 120 and ~ 220 km depth, respectively (Fig. 5). Based on stress-field inversion, Li et al. (2018b) estimated that σ_1 and σ_3 of Group I events are predominantly along ~ 150° strike, ~ 10° dip and ~ 30° strike, ~ 70° dip, respectively. Group II events, in contrast, show σ_1 with ~ 170° strike and ~ 10° dip and σ_3 with -40° strike and ~ 80° dip. These authors further argued that the two groups have different mechanisms. While metamorphic processes were proposed to be responsible for Group I events, subducted crustal materials to depths of 150-180 km were attributed to the low velocity and reduced seismicity between Group I and Group II. Stretching or detachment of the slab was proposed to induce earthquakes deeper than 200 km (Kufner et al., 2016; Zhan and Kanamori, 2016; Li et al., 2018b). In addition, aftershocks of IDEQs in the region share many common characteristics of the shallow earthquakes, such as anti-correlation with mainshock slip distribution (Fig. 5) and similar statistical behaviors, such as the Gutenberg-Richter *b* values and the Omori aftershock decay *p* values. These were used to argue that the common mechanisms responsible for shallow earthquakes may also apply for IDEQs (Li et al., 2018a).

Triggered events in and around Tibetan Plateau

Large earthquakes are known to trigger additional seismic events, either around the mainshock ruptures or at long distances (Freed, 2005; Hill and Prejean, 2015; King and Devès, 2015). The former category is generally known as aftershocks, while the latter is typically called remotely triggered earthquakes. Here we review recent evidence of triggered earthquakes around Tibetan Plateau, focusing primarily on microseismicity remotely triggered by large distant mainshocks.

Perhaps the most well-studied triggering mainshock is the 2004 M 9.3 Sumatra earthquake (Fig. 6a). It was the largest earthquake in the last 50 years and occurred at the subduction boundary between the India and Burma plates (Ammon et al., 2005). Following the mainshock, there was a sharp increase in microseismicity in Yunnan province, Southwestern China that last for ~ 14 days at distances ranging from 2000 to 3000 km (Fig. 6b), suggesting a remote triggering relationship (Lei et al., 2011; Peng et al., 2012; Li et al., 2019a). Most triggered events

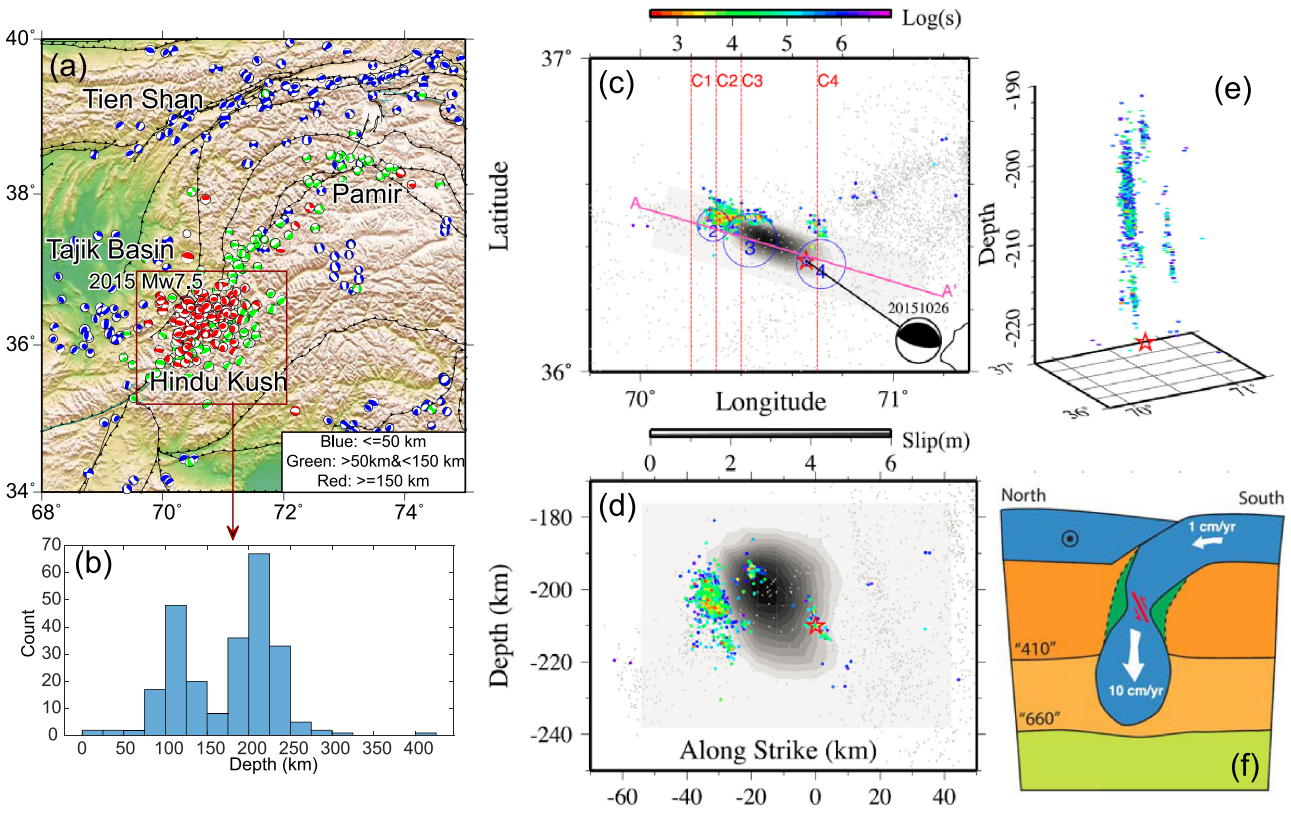

Figure 5. (a) Focal mechanisms in Hindu Kush. Beachball solutions are color-coded according to event depth: red (<50 km), green (50–150 km), and blue (>150 km). (b) earthquake occurrence rate (M > 4.5) as a function of depth. Note bimodal distribution. (c) Map view of background seismicity (gray) and aftershocks of the 2015 M 7.5 mainshock (Li et al., 2018a). The color of aftershocks is their relative time to the mainshock. The gray area and contours are slip distribution from the UGSS finite fault model. The blue circles mark subevents from (Zhan and Kanamori, 2016). AA' marks strike direction in panel (d). (d) A comparison of the mainshock slip distribution and aftershock location in the depth-profile. The red star marks the initial hypocenter of the 2015 M 7.5 mainshock. (e) A three-dimensional view of aftershocks. (f) A schematic diagram showing the slab tearing model for the generation of IDEQs in this region (Zhan and Kanamori, 2016).

were clustered in regions with complex fault geometries or volcanic activities (Lei et al., 2011). In fact, the first triggered event (magnitude 4.8) occurred in the Tengchong volcanic field during the Rayleigh wave pulses of the Sumatra mainshock (Lei et al., 2011) (Fig. 6c). The associated dynamic stresses of the Sumatra mainshock were on the order of 0.5 MPa (Li et al., 2019a), well above the typical remote triggering threshold of 5–10 KPa (Brodsky and Prejean, 2005; Aiken and Peng, 2014). Interestingly, ~ 8 years later, the M 8.6 Indian Ocean earthquake and its M 8.2 aftershock only triggered microseismicity in a few isolated regions (Li et al., 2019a), in stark contrast to the global increase of M > 5.5 earthquakes following the previous sequence (Pollitz et al., 2012). Li et al. (2019a) argued that perhaps the triggering threshold around Yunnan is rather high, and only the 2004 Sumatra mainshock was able to generate dynamic stress changes high enough to promote frictional failures and trigger microseismicity.

Yao et al. (2015) analyzed remote triggering in south-central Tibet following the 2004 M 9.3 Sumatra and the 2005 M 8.6 Nias earthquakes (Fig. 6a). This region is particularly interesting due to the existence of many N-S rift systems (normal faults; see Fig. 1a). In addition, a M 6.3 normal-faulting earthquake occurred near Zhongba (south of the BNS in the Lhasa Terrane), about 10 days after the Nias mainshock, raising speculation that the Zhongba earthquake was delayed-triggered by the Nias event (Ryder and Burgmann, 2011). Based on visual inspection of high-frequency signals and a template matching analysis, many triggered earthquakes were detected during and immediately following both the Sumatra and the Nias mainshocks (Figs. 6e–6g). Triggered seismicity occurred mostly north of the BNS in the Qiangtang Terrane and lasted ~ 50 hours and a few hours following the Sumatra the Nias mainshocks, respectively. Interestingly, no triggered microearthquakes were identified in the Zhongba region following the Nias mainshock and before the M 6.3 Zhongba event. These results suggest that some crustal faults in south-central Tibet are critically stressed, and they can easily respond to external stress perturbations from large distant earthquakes.

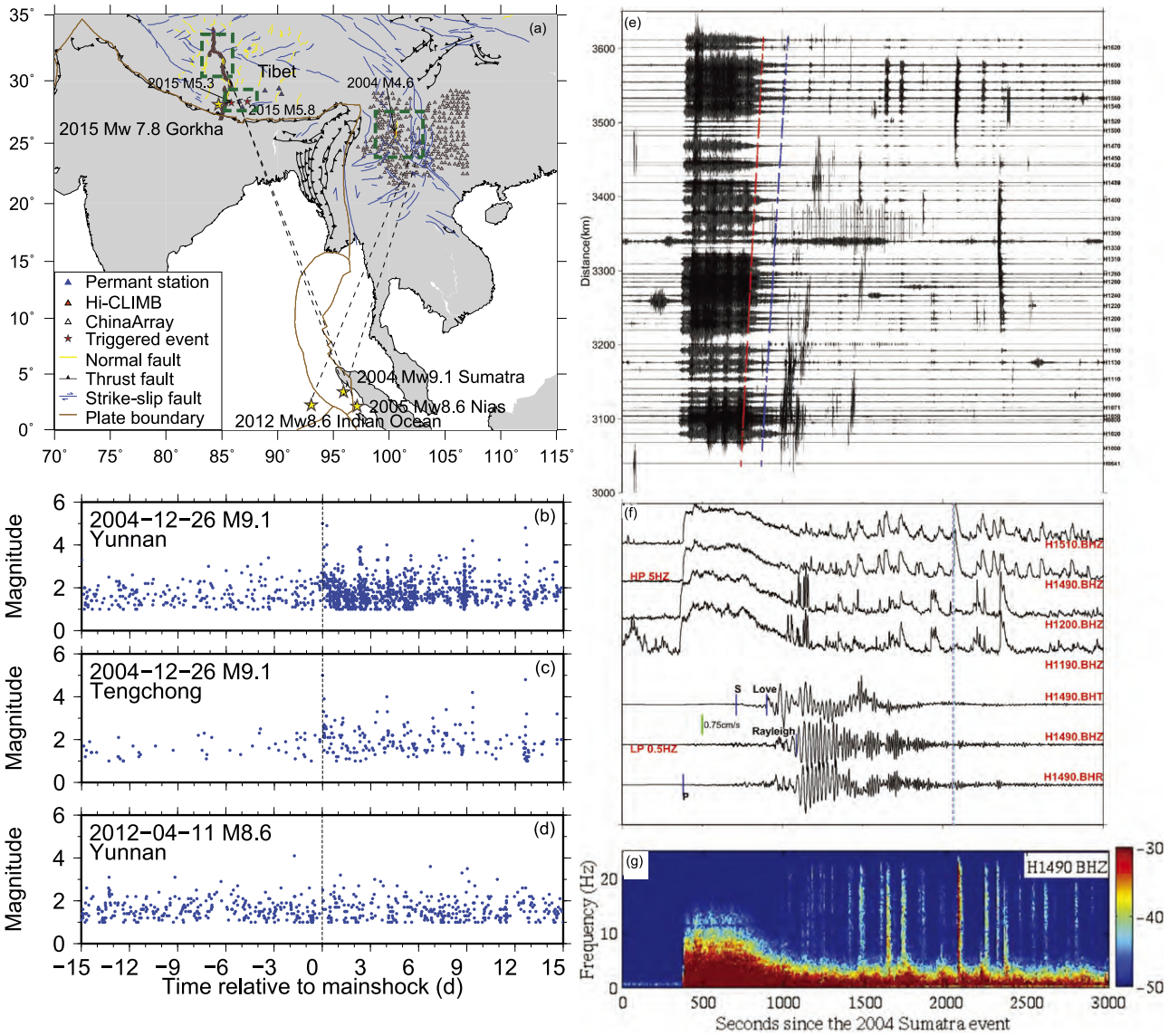

Figure 6. (a) A summary of triggered seismicity around Tibet following recent large earthquakes (after Yao et al., 2015 and Li et al. 2019a). The triggering mainshocks include the 2004 M 9.1 Sumatra, the 2005 M 8.6 Nias, and the 2012 M 8.6 Indian Ocean the 2015 M 7.8 Nepal earthquakes. The triggered sites are marked as green dashed boxes. (b)-(d) The seismicity changes within 15 days of the 2004 Sumatra and 2012 Indian Ocean mainshocks in Yunnan (b) and (d) and Tengchong region (c). (e) 5-Hz high-passed vertical-component waveforms recorded by the Hi-Climb array aligned with epicentral distances to the 2004 M_w 9.1 Sumatra mainshock. The dashed red and blue lines mark the predicted Love and Rayleigh wave arrival (with a nominal phase velocity of 4.1 and 3.5 km/s). (b) Log10 envelope function of 5-Hz high-passed seismograms at selected stations. The bottom three traces are broadband recordings rotating to transverse, vertical and radial components. *P*, *S*, Love and Rayleigh phases are marked. (c) Spectrogram of vertical component recorded at station H1490 showing triggered seismicity.

Li et al. (2017) performed a similar study in southern Tibet following the 2015 M 7.8 Gorkha, Nepal earthquake and found a clear increase in post mainshock seismicity, including two M > 5 normal-faulting events within the next half day (Fig. 6a). Because of the close distance, these authors were unable to distinguish two possible triggering mechanisms, i.e., static stress changes due to fault displacement versus dynamic stress changes due to passing seismic waves. Nevertheless, their study highlights the potential hazard of normal-faulting earthquakes in southern Tibet following major thrust-faulting earthquakes along the Himalaya frontal thrust faults. In addition, several large (M > 7) normal-faulting events were found elsewhere following the occurrence of megathrust earthquakes such as the 2006 M 8.3 Kuril Island, the 2010 M 8.8 Chile, and the 2011 M 9.1 Tohoku-Oki earthquakes (Ammon et al., 2008; Kato et al., 2011; Ryder et al., 2012). Hence, it is evident that active faults

around Tibet (and elsewhere) are interconnected and can be potentially triggered through either static or dynamic stress perturbations.

Due to limited station coverage and data availability, only a few studies focused on triggering of microseismicity along the Himalaya after large distant earthquakes. Mendoza et al. (2016) found clear evidence of local seismicity in central Himalaya triggered by long-period surface waves of the 2007 M 8.5 Sumatra earthquake. The associated peak dynamic stress is ~9 KPa, suggesting that faults along Himalaya are also sensitive to small stress changes.

Based on seismic catalogs from the National Seismological Center in Kathmandu, Nepal, Bollinger et al. (2007) reported that seismicity rates in winter is about 30–60% higher than that in summer months. Such seasonal variations of microseismicity is consistent with triggering due to surface load variations of annual hydrological cycle, for which the associated Coulomb stress changes are on the order of 2–4 kPa (Bettinelli et al., 2008). Ader and Avouac (2013) applied Schuster spectrum analysis to the same catalog and confirmed the existence of annual variation in seismicity rate, and a lack of variation in any other tidal periods. Wang et al. (2018) found an interesting anti-correlation between background seismicity and monthly precipitation in southwestern Longmenshan region. It may be interesting to compare these studies with those in other regions of the world. Heki (2003) reported that snow melt in inland Japan induced crustal earthquakes. Similarly, Johnson et al. (2017) found that microseismicity in Central California varies with seasonal water accumulation cycles, presumably due to loading variations of the hydrosphere onto the crust. These studies suggest that some faults are near a critical stage and can be triggered/modulated by long-term stress variations on the order of only a few kPa.

POSSIBLE MECHANISMS OF INTERMEDIATE-DEPTH SEISMICITY UNDER SOUTHERN TIBET

At depths below ~ 30 km, increasing isostatic pressure induces a brittle-ductile transition and rocks normally behave in a ductile manner (Brace and Kohlstedt, 1980). In addition, the temperature conditions at depths are such that plastic yield strength of rocks is well below Byerlee's frictional strength (Byerlee, 1978). Three hypotheses have been proposed to induce mechanical instability within the normally ductile regime. The first is a thermal runaway process where a self-amplifying mechanical instability arises from the combination of shear localization and grain size reduction within a visco-plastic material (Kelemen and Hirth, 2007; Thielmann, 2018). Crucial issue here is the conditions under which shear localizations nucleate and self-amplify, leading to failure (John et al., 2009). Such conditions are poorly known and have just begun to be investigated in the laboratory (Ohuchi et al., 2017). The second is dehydration embrittlement, in which a metamorphic dehydration reaction raises pore pressure, thereby lowering the effective pressure, permitting brittle failure (Raleigh and Paterson, 1965; Green and Houston, 1995; Dobson et al., 2002; Jung and Green, 2004). This hypothesis requires sufficient structural water in constituent minerals and is considered a good candidate for seismicity in subducted oceanic crust (Peacock, 2001; Ferrand et al., 2017). However, xenolith samples from Tibet suggest that the Indian lower crust lacks hydrous minerals (Hacker et al., 2000), making this mechanism less likely to operate under southern Tibet. The third is eclogitization-induced instability (Kirby et al., 1996; Jackson et al., 2004; Zhang et al., 2004a). The Indian shield consists predominantly of granulite-facies rocks, whose major minerals are pyroxenes (Pyx), plagioclase (Plg), and quartz (Gupta et al., 2003; Priestley et al., 2008). As such rocks are brought down to below 50–60 km depth through subduction, metamorphic transformation takes place (Liou et al., 1994). Seismic and gravity anomaly data support the existence of eclogite in subducted Indian crust (Schulte-Pelkum et al., 2005; Hetényi et al., 2007; Wittlinger et al., 2009; Zhang et al., 2014, Gilligan et al., 2015) and eclogite xenoliths have been found in central Tibet (Yang et al., 2009; Dong et al., 2016). Pseudotachylytes, usually formed by brittle failure followed by frictional melting during shallow seismicity, are found in exhumed deep continental rocks in western Norway (Austrheim and Boundy, 1994). These dominantly granulite facies rocks contain eclogite facies minerals in close association with the pseudotachylytes, suggesting that granulite-facies rocks may have transformed partially at depths, under conditions corresponding to the eclogite facies stability field. Some advocated that deep crustal seismicity under southern Tibet may be analogous to that in western Norway (Jackson et al., 2004). Others argue that eclogitization involves reconstructive phase transformations in constituent minerals and is unlikely to trigger mechanical instability (Green and Houston, 1995).

In a series of experimental investigation, Shi et al. (2018) and Incel et al. (2019) deformed granulite rocks under various pressure (P) and temperature (T) conditions within both granulite and eclogite stability fields, to examine the micro-mechanics responsible for rupture nucleation and self-organization leading to macroscopic faulting. By combining synchrotron X-ray diffraction and

imaging for stress and strain measurements with acoustic emission (AE) monitoring, they showed that eclogitization of metastable granulite indeed induces mechanical instability in the laboratory. The samples studied by Shi et al. (2018) were pre-sintered synthetic dry mafic granulite. The samples studied by Incel et al. (2019) were natural (hydrous) granulite from Holsnøy, southwestern Norway. Using advanced seismological tools such as the double-difference relocation program hypoDD (Waldhauser and Ellsworth, 2000), Shi et al. (2018) located the AE events, and tracked faulting process in both space and time. When dry granulite samples were deformed in the granulite-facies field, they displayed only ductile behavior and produced no AE events. In contrast, both dry and hydrous granulite samples deformed in the eclogite-facies field radiated numerous AEs and failed with large stress drops within a narrow temperature range from ~ 1000 to ~ 1300 K. Above and below this range, samples were ductile. Recovered dry samples from between 1073 and 1273 K contained conjugated macroscopic faults (Fig. 7). The brittle response is therefore clearly due to eclogitization of metastable granulite. In fact, such metamorphism-induced embrittlement occurs in wet system as well (Incel et al., 2019).

Based on the experimental observations, a micromechanical model of rupture nucleation and propagation is proposed (Figs. 7a and 7b). As the initially equilibrium granulite-facies mineral assemblage (Fig. 7a) is brought down by subduction process into the eclogite-facies stability field, Plg breaks down and reacts with Pyx. In the Plg breakdown reaction, anorthite and albite transform to grossular + kyanite + quartz and jadeite + quartz, respectively, while in the Plg-Pyx reaction, omphacite and quartz are formed. Experimentally, both reactions produce thin bands consisting of nanograined reaction products, termed nano-reaction bands (NRBs) (Fig. 7b). Under shear stress, these NRBs form within Plg grains and along grain interfaces, weakening the rock assembly and causing micro-ruptures. The heat released by the exothermic reactions involved further enhanced rate of transformation, producing ultra-fine-grained reaction product (Incel et al., 2019). Together, these effects induce strain localization and mechanical instability. These authors argue that eclogitization-induced embrittlement provides a viable mechanism for IDEQs in the lower crust under southern Tibet.

Sub-Moho earthquakes in southern Tibet tend to be clustered in close proximity to events in the lower crust (Monsalve et al., 2006). Mechanisms for the seismicity below the Moho remain unresolved. The dominant minerals in the upper mantle are olivine and Pyx. A recent study shows that at pressures corresponding to depths up

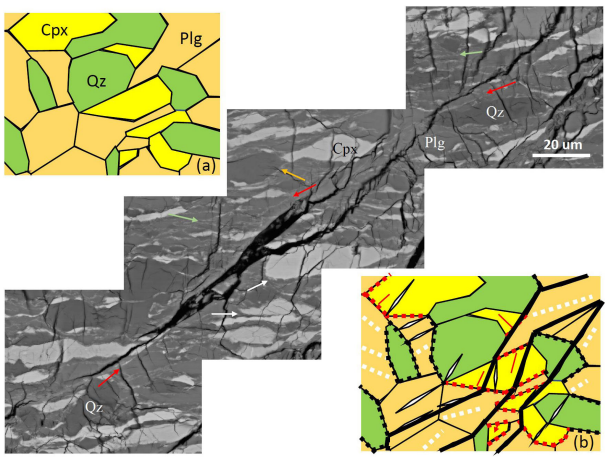

Figure 7. A micromechanical model of mechanical instability induced by eclogitization of granulite. The center figure is a composite back-scattered SEM image of recovered granulite sample deformed at 2.8 GPa and 1073 K, showing a major fault running from upper right to lower left. Maximum compressive stress direction is vertical in this triaxial deformation experiment. Near vertical cracks were due to decompression. Three phases are clearly visible with different brightness. The brightest phase is clinopyroxene (Cpx), intermediate grey is plagioclase (Plg), and the darkest phase is quartz (Qz). Note extensive faults cutting through grains of different mineralogy. Within Plg, numerous thin bright bands are present, as indicated by red and light green arrows. These nano-reaction bands (NRBs) contain products of Plg breakdown reaction (Shi et al., 2018). Similar NRBs can be seen around Cpx (white arrow) and Qz (orange arrow) grains which are bounded with Plg. Cartoon illustration (a) shows a typical microstructure before the eclogitization reaction and (b) after syn-deformational eclogitization. White dotted lines represent NRBs in Plg, red and black dotted lines represent NRBs on the Cpx and Qz grain boundaries adjacent to Plg grains. Thick black lines illustrate self-organization of these NRBs, forming large-scale faults.

to 100 km, shear-banding and localized heating may develop in deforming olivine, resulting in seismogenic faulting (Ohuchi et al., 2017). Numerical modeling also shows that as deformation mechanisms change (either due to temperature or stress), shear localization may develop and may cause potential adiabatic heating, inducing mechanical instability (Thielmann, 2018). From these viewpoints, sub-Moho seismicity under southern Tibet may be interpreted as shear-localization induced instability triggered by stress heterogeneities produced through strong mechanical coupling between the crust and upper mantle.

CONCLUSIONS

The Himalayas and Tibetan Plateau are the most tectonically active continental convergent regions, where numerous earthquakes have occurred. Shallow events (focal

depths <50 km) show remarkable correlation with surface fault systems in both spatial location and focal mechanisms. Some shallow events appear to be triggered by remote earthquakes, suggesting stress levels are near critical threshold. There is indication that even seasonal monsoon cycles may trigger some events. IDEQs are concentrated in southern Tibet, the Hindu Kush–Pamir region, and the Burmese subductions zone. Underneath southern Tibet, the subducted Indian plate extends northward to at least the Bangong–Nujiang suture zone, with IDEQs occurring in the lower crust and the adjacent upper mantle. Possible mechanisms for IDEQs are elclogitization–induced embrittlement in the subducted Indian lower crust and shear–localization in the upper mantle.

ACKNOWLEDGMENTS

We thank A. Baranov for providing his Moho model data, based on which Figure 2 was created, and H. Jung and an anonymous reviewer for constructive comments. This work was partially supported by the US National Science Foundation EAR–1661489 and 1925920 (to Y.W.), EAR–1925165 (to Z.P.), and the Youth Innovation Promotion Association of CAS (to Y.D.).

REFERENCES

Ader, T.J. and Avouac, J.–P. (2013) Detecting periodicities and declustering in earthquake catalogs using the Schuster spectrum, application to Himalayan seismicity. Earth and Planetary Science Letters, 377–378, 97–105.

Aiken, C. and Peng, Z. (2014) Dynamic triggering of microearthquakes in three geothermal/volcanic regions of California. Journal of Geophysical Research: Solid Earth, 119, 6992–7009.

Ammon, C.J., Ji, C., Thio, H.–K., Robinson, D., et al. (2005) Rupture Process of the 2004 Sumatra–Andaman Earthquake. Science, 308, 1133–1139.

Ammon, C.J., Kanamori, H. and Lay, T. (2008) A great earthquake doublet and seismic stress transfer cycle in the central Kuril islands. Nature, 451, 561.

Angelier, J. and Baruah, S. (2009) Seismotectonics in Northeast India: a stress analysis of focal mechanism solutions of earthquakes and its kinematic implications. Geophysical Journal International, 178, 303–326.

Austrheim, H. and Boundy, T.M. (1994) Pseudotachylytes generated during seismic faulting and eclogitization of the deep crust. Science, 265, 82–83.

Avouac, J.P. (2015) Mountain building: From earthquakes to geologic deformation. In Treatise on Geophysics (Second Edition) (Schubert, G. Ed.), 6. Elsevier, Oxford, 381–432.

Bai, L., Li, G., Khan, N.G., Zhao, J., et al. (2017) Focal depths and mechanisms of shallow earthquakes in the Himalayan–Tibetan region. Gondwana Research, 41, 390–399.

Baranov, A., Bagherbandi, M. and Tenzer, R. (2018) Combined Gravimetric–Seismic Moho Model of Tibet. Geosciences, 8, 461.

Bettinelli, P., Avouac, J.–P., Flouzat, M., Bollinger, L., et al. (2008) Seasonal variations of seismicity and geodetic strain in the Himalaya induced by surface hydrology. Earth and Planetary Science Letters, 266, 332–344.

Bilham, R. and England, P. (2001) Plateau 'pop–up' in the great 1897 Assam earthquake. Nature, 410, 806–809.

Bollinger, L., Perrier, F., Avouac, J.–P., Sapkota, S., et al. (2007) Seasonal modulation of seismicity in the Himalaya of Nepal. Geophysical Research Letters, 34, L08304.

Brace, W.F. and Kohlstedt, D.L. (1980) Limits on lithospheric stress imposed by laboratory experiments. Journal of Geophysical Research: Solid Earth, 85, 6248–6252.

Brodsky, E.E. and Prejean, S.G. (2005) New constraints on mechanisms of remotely triggered seismicity at Long Valley Caldera. Journal of Geophysical Research: Solid Earth, 110, B04302.

Byerlee, J. (1978) Friction of rocks. Pure and Applied Geophysics, 116, 615–626.

Ceylan, S., Ni, J., Chen, J.Y., Zhang, Q., et al. (2012) Fragmented Indian plate and vertically coherent deformation beneath eastern Tibet. Journal of Geophysical Research: Solid Earth, 117, B11303.

Chen, M., Niu, F., Tromp, J., Lenardic, A., et al. (2017) Lithospheric foundering and underthrusting imaged beneath Tibet. Nature Communications, 8, 15659.

Chen, W.–P. and Molnar, P. (1983) Focal depths of intracontinental and intraplate earthquakes and their implications for the thermal and mechanical properties of the lithosphere. Journal of Geophysical Research: Solid Earth, 88, 4183–4214.

Chen, W.–P. and Molnar, P. (1990) Source parameters of earthquakes and intraplate deformation beneath the Shillong Plateau and the Northern Indoburman Ranges. Journal of Geophysical Research: Solid Earth, 95, 12527–12552.

Chen, W.–P. and Yang, Z. (2004) Earthquakes beneath the Himalayas and Tibet: Evidence for strong lithospheric mantle. Science, 304, 1949–1952.

Chen, W.–P., Martin, M., Tseng, T.–L., Nowack, R.L., et al. (2010) Shear–wave birefringence and current configuration of converging lithosphere under Tibet. Earth and Planetary Science Letters, 295, 297–304.

Chen, Y., Li, W., Yuan, X., Badal, J., et al. (2015) Tearing of the Indian lithospheric slab beneath southern Tibet revealed by SKS–wave splitting measurements. Earth and Planetary Science Letters, 413, 13–24.

Copley, A., Avouac, J.–P. and Wernicke, B.P. (2011) Evidence for mechanical coupling and strong Indian lower crust beneath southern Tibet. Nature, 472, 79–81.

Craig, T.J., Copley, A. and Jackson, J. (2012) Thermal and tectonic consequences of India underthrusting Tibet. Earth and Planetary Science Letters, 353–354, 231–239.

Cui, Z., Chen, Z., Wang, Q. and Li, J. (2019) Characteristics of focal mechanism and stress in the North–South Seismic Belt of China. Earthquakes, 39, 1–10 (in Chinese with English abstract).

De La Torre, T.L., Monsalve, G., Sheehan, A.F., Sapkota, S., et al. (2007) Earthquake processes of the Himalayan collision zone in eastern Nepal and the southern Tibetan Plateau. Geophysical Journal International, 171, 718–738.

Deng, Y. and Tesauro, M. (2016) Lithospheric strength variations in Mainland China: Tectonic implications. Tectonics, 35, 2313–2333.

Deng, Y., Li, J., Song, X. and Zhu, L. (2018) Joint inversion for lithospheric structures: Implications for the growth and deformation in northeastern Tibetan Plateau. Geophysical Research Letters, 45, 3951–3958.

Dobson, D.P., Meredith, P.G. and Boon, S.A. (2002) Simulation of subduction zone seismicity by dehydration of serpentine. Science, 298, 1407–1410.

Dong, Y.-L., Wang, B.-D., Zhao, W.-X., Yang, T.-N., et al. (2016) Discovery of eclogite in the Bangong Co-Nujiang ophiolitic mélange, central Tibet, and tectonic implications. Gondwana Research, 35, 115–123.

Ekström, G., Nettles, M. and Dziewonski, A.M. (2012) The global CMT project 2004–2010: Centroid-moment tensors for 13,017 earthquakes. Physics of Earth and Planetary Interior, 200–201, 1–9.

Engdahl, E.R., van der Hilst, R. and Buland, R. (1998) Global teleseismic earthquake relocation with improved travel times and procedures for depth determination. Bulletin of the Seismological Society of America, 88, 722–743.

Ferrand, T.P., Hilairet, N., Incel, S., Deldicque, D., et al. (2017) Dehydration-driven stress transfer triggers intermediate-depth earthquakes. Nature Communications, 8, 15247.

Freed, A.M. (2005) Earthquake triggering by static, dynamic, and postseismic stress transfer. Annual Review of Earth and Planetary Sciences, 33, 335–367.

Gan, W., Zhang, P., Shen, Z.-K., Niu, Z., et al. (2007) Present-day crustal motion within the Tibetan Plateau inferred from GPS measurements. Journal of Geophysical Research: Solid Earth, 112, B08416.

Gao, Y., Wang, Q., Zhao, B. and Shi, Y. (2014) A rupture blank zone in middle south part of Longmenshan Faults: Effect after Lushan M_S 7.0 earthquake of 20 April 2013 in Sichuan, China. Science China Earth Sciences, 57, 2036.

Gilligan, A., Priestley, K.F., Roecker, S.W., Levin, V., et al. (2015) The crustal structure of the western Himalayas and Tibet. Journal of Geophysical Research: Solid Earth, 120, B011891.

Green, H.W. and Houston, H. (1995) The mechanics of deep earthquakes. Annual Review of Earth and Planetary Sciences, 23, 169–213.

Grujic, D. (2006) Channel flow and continental collision tectonics: an overview. Geological Society, London, Special Publications, 268, 25–37.

Gupta, S., Rai, S.S., Prakasam, K.S., Srinagesh, D., et al. (2003) The nature of the crust in southern India: Implications for Precambrian crustal evolution. Geophysical Research Letters, 30, 1419.

Hacker, B.R., Gnos, E., Ratschbacher, L., Grove, M., et al. (2000) Hot and dry deep crustal xenoliths from Tibet. Science, 287, 2463–2466.

Harris, N. (2007) Channel flow and the Himalayan-Tibetan orogen: a critical review. Journal of the Geological Society, 164, 511–523.

Heki, K. (2003) Snow load and seasonal variation of earthquake occurrence in Japan. Earth and Planetary Science Letters, 207, 159–164.

Hetényi, G., Cattin, R., Brunet, F., Bollinger, L., et al. (2007) Density distribution of the India plate beneath the Tibetan plateau: Geophysical and petrological constraints on the kinetics of lower-crustal eclogitization. Earth and Planetary Science Letters, 264, 226–244.

Hetényi, G., Vergne, J., Bollinger, L. and Cattin, R. (2011) Discontinuous low-velocity zones in southern Tibet question the viability of the channel flow model. Geological Society, London, Special Publications, 353, 99–108.

Hill, D.P. and Prejean, S.G. (2015) Dynamic Triggering. In Treatise on Geophysics (Second Edition) (Schubert, G. Ed.), 4. Elsevier, Oxford, 273–304.

Huang, W.-C., Ni, J.F., Tilmann, F., Nelson, D., et al. (2000) Seismic polarization anisotropy beneath the central Tibetan Plateau. Journal of Geophysical Research: Solid Earth, 105, 27979–27989.

Incel, S., Labrousse, L., Hilairet, N., John, T., et al. (2019) Reaction-induced embrittlement of the lower continental crust. Geology, 47, 235–238.

Jackson, J. (2002) Strength of the continental lithosphere: Time to abandon the jelly sandwich?. GSA Today, 12, 4–10.

Jackson, J.A., Austrheim, H., McKenzie, D. and Priestley, K. (2004) Metastability, mechanical strength, and the support of mountain belts. Geology, 32, 625–628.

Jiang, M., Zhou, S., Sandvol, E., Chen, X., et al. (2011) 3-D lithospheric structure beneath southern Tibet from Rayleigh-wave tomography with a 2-D seismic array. Geophysical Journal International, 185, 593–608.

Jiménez-Munt, I., Fernàndez, M., Vergés, J. and Platt, J.P. (2008) Lithosphere structure underneath the Tibetan Plateau inferred from elevation, gravity and geoid anomalies. Earth and Planetary Science Letters, 267, 276–289.

John, T., Medvedev, S., Rupke, L.H., Andersen, T.B., et al. (2009) Generation of intermediate-depth earthquakes by self-localizing thermal runaway. Nature Geoscience, 2, 137–140.

Johnson, C.W., Fu, Y. and Bürgmann, R. (2017) Seasonal water storage, stress modulation, and California seismicity. Science, 356, 1161–1164.

Jordan, T.A. and Watts, A.B. (2005) Gravity anomalies, flexure and the elastic thickness structure of the India-Eurasia collisional system. Earth and Planetary Science Letters, 236, 732–750.

Jung, H. and Green, H.W. (2004) Experimental faulting of serpentinite during dehydration: Implications for earthquakes, seismic low-velocity zones, and anomalous hypocenter distributions in subduction zones. International Geology Review, 46, 1089–1102.

Kapp, P. and Guynn, J.H. (2004) Indian punch rifts Tibet. Geology, 32, 993–996.

Kato, A., Sakai, S. and Obara, K. (2011) A normal-faulting seismic sequence triggered by the 2011 off the Pacific coast of Tohoku Earthquake: Wholesale stress regime changes in the upper plate. Earth, Planets and Space, 63, 43.

Kelemen, P.B. and Hirth, G. (2007) A periodic shear-heating mechanism for intermediate-depth earthquakes in the mantle. Nature, 446, 787–790.

Khan, P.K. (2005) Variation in dip-angle of the Indian plate subducting beneath the Burma plate and its tectonic implications. Geoscience Journal, 9, 227–234.

Kind, R., Yuan, X., Saul, J., Nelson, D., et al. (2002) Seismic images of crust and upper mantle beneath Tibet: Evidence for Eurasian plate subduction. Science, 298, 1219–1221.

Kind, R. and Yuan, X. (2010) Seismic Images of the Biggest Crash on Earth. Science, 329, 1479–1480.

King, G.C.P. and Devès, M.H. (2015) Fault Interaction, Earthquake Stress Changes, and the Evolution of Seismicity. In: Treatise on Geophysics (Second Edition) (Schubert, G. Ed.), 4. Elsevier, Oxford, 243–271.

Kirby, S.H., Engdahl, E.R. and Denlinger, R. (1996) Intermediate-depth intraslab earthquakes and arc volcanism as physical ex-

pressions of crustal and uppermost mantle metamorphism in subducting slabs. In: Subduction: Top to Bottom (Bebout, G.E. et al. Eds.). Geophysical Monograph Series 96, American Geophysical Union, Washington, DC, 195–214.

Kufner, S.-K., Schurr, B., Sippl, C., Yuan, X., et al. (2016) Deep India meets deep Asia: Lithospheric indentation, delamination and break-off under Pamir and Hindu Kush (Central Asia). Earth and Planetary Science Letters, 435, 171–184.

Kufner, S.-K., Schurr, B., Haberland, C., Zhang, Y., et al. (2017) Zooming into the Hindu Kush slab break-off: A rare glimpse on the terminal stage of subduction. Earth and Planetary Science Letters, 461, 127–140.

Kumar, A., Mitra, S. and Suresh, G. (2015) Seismotectonics of the eastern Himalayan and indo-burman plate boundary systems. Tectonics, 34, 2279–2295.

Kumar, P., Yuan, X., Kind, R. and Ni, J. (2006) Imaging the colliding Indian and Asian lithospheric plates beneath Tibet. Journal of Geophysical Research: Solid Earth, 111, B06308.

Lei, X., Xie, C. and Fu, B. (2011) Remotely triggered seismicity in Yunnan, southwestern China, following the 2004 M_w 9.3 Sumatra earthquake. Journal of Geophysical Research: Solid Earth, 116, B08303.

Li, C., van der Hilst, R. and Meltzer, A. (2008) Subduction of the Indian lithosphere beneath the Tibetan Plateau and Burma. Earth and Planetary Science Letters, 274, 157–168.

Li, C., Peng, Z., Yao, D., Guo, H., et al. (2018a) Abundant aftershock sequence of the 2015 M_w7.5 Hindu Kush intermediate-depth earthquake. Geophysical Journal International, 213, 1121–1134.

Li, J. and Song, X. (2018) Tearing of Indian mantle lithosphere from high-resolution seismic images and its implications for lithosphere coupling in southern Tibet. Proceedings of the National Academy of Sciences, 115, 8296–8300.

Li, L., Yao, D., Meng, X., Peng, Z., et al. (2017) Increasing seismicity in Southern Tibet following the 2015 M_w7.8 Gorkha, Nepal earthquake. Tectonophysics, 714–715, 62–70.

Li, L., Wang, B., Peng, Z. and Li, D. (2019a) Dynamic triggering of microseismicity in Southwest China following the 2004 Sumatra and 2012 Indian Ocean earthquakes. Journal of Asian Earth Sciences, 176, 129–140.

Li, W., Chen, Y., Yuan, X., Schurr, B., et al. (2018b) Continental lithospheric subduction and intermediate-depth seismicity: Constraints from S-wave velocity structures in the Pamir and Hindu Kush. Earth and Planetary Science Letters, 482, 478–489.

Li, X., Wei, D., Yuan, X., Kind, R., et al. (2011) Details of the doublet Moho structure beneath Lhasa, Tibet, obtained by comparison of P and S receiver functions. Bulletin of the Seismological Society of America, 101, 1259–1269.

Li, X., Hergert, T., Henk, A., Wang, D., et al. (2019b) Subsurface structure and spatial segmentation of the Longmen Shan fault zone at the eastern margin of Tibetan Plateau: Evidence from focal mechanism solutions and stress field inversion. Tectonophysics, 757, 10–23.

Liang, C. and Song, X. (2006) A low velocity belt beneath northern and eastern Tibetan Plateau from Pn tomography. Geophysical Research Letters, 33, L22306.

Liang, X., Zhou, S., Chen, Y.J., Jin, G., et al. (2008) Earthquake distribution in southern Tibet and its tectonic implications. Journal of Geophysical Research: Solid Earth, 113, B12409.

Liang, X., Chen, Y., Tian, X., Chen, Y.J., et al. (2016) 3D imaging of subducting and fragmenting Indian continental lithosphere beneath southern and central Tibet using body-wave finite-frequency tomography. Earth and Planetary Science Letters, 443, 162–175.

Liou, J.G., Zhang, R. and Ernst, W.G. (1994) An introduction to ultrahigh-pressure metamorphism. Island Arc, 3, 1–24.

Liu, Z., Tian, X., Gao, R., Wang, G., et al. (2017) New images of the crustal structure beneath eastern Tibet from a high-density seismic array. Earth and Planetary Science Letters, 480, 33–41.

Liu, Z., Liang, C., Hua, Q., Li, Y., et al. (2018) The seismic potential in the seismic gap between the Wenchuan and Lushan earthquakes revealed by the joint inversion of receiver functions and ambient noise data. Tectonics, 37, 4226–4238.

Maggi, A., Jackson, J.A., McKenzie, D. and Priestley, K. (2000) Earthquake focal depths, effective elastic thickness, and the strength of the continental lithosphere. Geology, 28, 495–498.

Mahmood, I., Kidwai, A.A., Qureshi, S.N., Iqbal, M.F., et al. (2015) Revisiting major earthquakes in Pakistan. Geology Today, 31, 33–38.

McNamara, D.E., Walter, W.R., Owens, T.J. and Ammon, C.J. (1997) Upper mantle velocity structure beneath the Tibetan Plateau from Pn travel time tomography. Journal of Geophysical Research: Solid Earth, 102, 493–505.

Mechie, J., Kind, R. and Saul, J. (2011) The seismological structure of the Tibetan Plateau crust and mantle down to 700 km depth. Geological Society, London, Special Publications, 353, 109–125.

Mendoza, M.M., Ghosh, A. and Rai, S.S. (2016) Dynamic triggering of small local earthquakes in the central Himalaya. Geophysical Research Letters, 43, 9581–9587.

Molnar, P. and Lyon-Caen, H. (1989) Fault plane solutions of earthquakes and active tectonics of the Tibetan Plateau and its margins. Geophysical Journal International, 99, 123–153.

Monsalve, G., Sheehan, A., Schulte-Pelkum, V., Rajaure, S., et al. (2006) Seismicity and one-dimensional velocity structure of the Himalayan collision zone: Earthquakes in the crust and upper mantle. Journal of Geophysical Research: Solid Earth, 111, B10301.

Nábělek, J., Hetényi, G., Vergne, J., Sapkota, S., et al. (2009) Underplating in the Himalaya-Tibet collision zone revealed by the Hi-CLIMB experiment. Science, 325, 1371–1374.

Nelson, K.D., Zhao, W., Brown, L.D., Kuo, J., et al. (1996) Partially molten middle crust beneath Southern Tibet: Synthesis of project INDEPTH results. Science, 274, 1684–1688.

Ohuchi, T., Lei, X., Ohfuji, H., Higo, Y., et al. (2017) Intermediate-depth earthquakes linked to localized heating in dunite and harzburgite. Nature Geoscience, 10, 771–776.

Peacock, S.M. (2001) Are the lower planes of double seismic zones caused by serpentine dehydration in subducting oceanic mantle?. Geology, 29, 299–302.

Pei, S., Zhang, H., Su, J. and Cui, Z. (2014) Ductile gap between the Wenchuan and Lushan Earthquakes revealed from the two-dimensional Pg seismic tomography. Scientific Reports, 4, 6489.

Peng, Y., Zhou, S., Zhuang, J. and Shi, J. (2012) An approach to detect the abnormal seismicity increase in Southwestern China triggered co-seismically by 2004 Sumatra Mw 9.2 earthquake. Geophysical Journal International, 189, 1734–1740.

Pollitz, F.F., Stein, R.S., Sevilgen, V. and Bürgmann, R. (2012) The 11 April 2012 east Indian Ocean earthquake triggered large aftershocks worldwide. Nature, 490, 250.

Priestley, K., Jackson, J. and McKenzie, D. (2008) Lithospheric structure and deep earthquakes beneath India, the Himalaya

and southern Tibet. Geophysical Journal International, 172, 345-362.

Prieto, G.A., Beroza, G.C., Barrett, S.A., López, G.A., et al. (2012) Earthquake nests as natural laboratories for the study of intermediate-depth earthquake mechanics. Tectonophysics, 570-571, 42-56.

Raleigh, C.B. and Paterson, M.S. (1965) Experimental deformation of serpentinite and its tectonic implications. Journal of Geophysical Research, 70, 3965-3985.

Rehman, K., Ali, A., Ahmed, S., Ali, W., et al. (2015) Spatio-temporal variations of b-value in and around north Pakistan. Journal of Earth System Science, 124, 1445-1456.

Rehman, K., Ali, W., Ali, A., Ali, A., et al. (2017) Shallow and intermediate depth earthquakes in the Hindu Kush region across the Afghan-Pakistan border. Journal of Asian Earth Sciences, 148, 241-253.

Royden, L. (1996) Coupling and decoupling of crust and mantle in convergent orogens: Implications for strain partitioning in the crust. Journal of Geophysical Research: Solid Earth, 101, 17679-17705.

Ryder, I. and Burgmann, R. (2011) Communication between multiple large earthquakes at different spatial scales across and beyond the Tibetan Plateau. American Geophysical Union Fall Meeting, Abstract #S21D-07.

Ryder, I., Rietbrock, A., Kelson, K., Bürgmann, R., et al. (2012) Large extensional aftershocks in the continental forearc triggered by the 2010 Maule earthquake, Chile. Geophysical Journal International, 188, 879-890.

Schulte-Pelkum, V., Monsalve, G., Sheehan, A., Pandey, M.R., et al. (2005) Imaging the Indian subcontinent beneath the Himalaya. Nature, 435, 1222-1225.

Schulte-Pelkum, V., Monsalve, G., Sheehan, A.F., Shearer, P., et al. (2019) Mantle earthquakes in the Himalayan collision zone. Geology, 47, 815-819.

Schurr, B., Ratschbacher, L., Sippl, C., Gloaguen, R., et al. (2014) Seismotectonics of the Pamir. Tectonics, 33, 1501-1518.

Searle, M.P., Law, R.D. and Jessup, M.J. (2006) Crustal structure, restoration and evolution of the Greater Himalaya in Nepal-South Tibet: implications for channel flow and ductile extrusion of the middle crust. Geological Society, London, Special Publications, 268, 355-378.

Shao, C., Liu, S., Li, Y., Zhou, R., et al. (2019) Paleoseismic events on the Shuangshi-Dachuan fault of the seismic gap, Longmen Shan thrust belt, eastern margin of the Tibetan Plateau. Journal of Asian Earth Sciences, 169, 1-10.

Sheehan, A., de La Torre, T.L., Monsalve, G., Schulte-Pelkum, V., et al. (2008) Earthquakes and crustal structure of the Himalaya from the Himalayan Nepal Tibet Seismic Zexperiment (HIMNT). Journal of Nepal Geological Society, 38, 1-8.

Shen, W., Ritzwoller, M.H., Kang, D., Kim, Y., et al. (2016) A seismic reference model for the crust and uppermost mantle beneath China from surface wave dispersion. Geophysical Journal International, 206, 954-979.

Shi, F., Wang, Y., Yu, T., Zhu, L., et al. (2018) Lower-crustal earthquakes in southern Tibet are linked to eclogitization of dry metastable granulite. Nature Communications, 9, 3483.

Sloan, R.A., Jackson, J.A., McKenzie, D. and Priestley, K. (2011) Earthquake depth distributions in central Asia, and their relations with lithosphere thickness, shortening and extension. Geophysical Journal International, 185, 1-29.

Su, T., Farnsworth, A., Spicer, R.A., Huang, J., et al. (2019) No high Tibetan Plateau until the Neogene. Science Advances, 5, eaav2189.

Tao, W. and Shen, Z. (2008) Heat flow distribution in Chinese continent and its adjacent areas. Progress in Natural Science, 18, 843-849.

Taylor, M. and Yin, A. (2009) Active structures of the Himalayan-Tibetan orogen and their relationships to earthquake distribution, contemporary strain field, and Cenozoic volcanism. Geosphere, 5, 199-214.

Thielmann, M. (2018) Grain size assisted thermal runaway as a nucleation mechanism for continental mantle earthquakes: Impact of complex rheologies. Tectonophysics, 746, 611-623.

Tilmann, F. and Ni, J. (2003) Seismic Imaging of the Downwelling Indian Lithosphere Beneath Central Tibet. Science, 300, 1424-1427.

Vergne, J., Wittlinger, G., Hui, Q., Tapponnier, P., et al. (2002) Seismic evidence for stepwise thickening of the crust across the NE Tibetan plateau. Earth and Planetary Science Letters, 203, 25-33.

Waldhauser, F. and Ellsworth, W.L. (2000) A double-difference earthquake location Algorithm: method and application to the Northern Hayward Fault, California. Bulletin of the Seismological Society of America, 90, 1353-1368.

Wang, C.-Y., Chen, W.-P. and Wang, L.-P. (2013) Temperature beneath Tibet. Earth and Planetary Science Letters, 375, 326-337.

Wang, C., Liang, C., Deng, K., Huang, Y., et al. (2018) Spatiotemporal distribution of microearthquakes and implications around the seismic gap between the Wenchuan and Lushan earthquakes. Tectonics, 37, 2695-2709.

Watts, A.B. and Burov, E.B. (2003) Lithospheric strength and its relationship to the elastic and seismogenic layer thickness. Earth and Planetary Science Letters, 213, 113-131.

Wittlinger, G., Farra, V., Hetényi, G., Vergne, J., et al. (2009) Seismic velocities in Southern Tibet lower crust: a receiver function approach for eclogite detection. Geophysical Journal International, 177, 1037-1049.

Yang, J., Xu, Z., Li, Z., Xu, X., et al. (2009) Discovery of an eclogite belt in the Lhasa block, Tibet: A new border for Paleo-Tethys?. Journal of Asian Earth Sciences, 34, 76-89.

Yang, Y., Liang, C., Li, Z., Su, J., et al. (2017) Stress distribution near the seismic gap between Wenchuan and Lushan earthquakes. Pure and Applied Geophysics, 174, 2257-2267.

Yao, D., Peng, Z. and Meng, X. (2015) Remotely triggered earthquakes in South-Central Tibet following the 2004 M_w 9.1 Sumatra and 2005 M_w 8.6 Nias earthquakes. Geophysical Journal International, 201, 543-551.

Ye, Z., Gao, R., Li, Q., Zhang, H., et al. (2015) Seismic evidence for the North China plate underthrusting beneath northeastern Tibet and its implications for plateau growth. Earth and Planetary Science Letters, 426, 109-117.

Yin, A. (2000) Mode of Cenozoic east-west extension in Tibet suggesting a common origin of rifts in Asia during the Indo-Asian collision. Journal of Geophysical Research: Solid Earth, 105, 21745-21759.

Yin, A., Grove, M., Murphy, M.A., Nie, S., et al. (1999) Tertiary deformation history of southeastern and southwestern Tibet during the Indo-Asian collision. GSA Bulletin, 111, 1644-1664.

Yin, A. and Harrison, T.M. (2000) Geologic Evolution of the Himalayan-Tibetan Orogen. Annual Review of Earth and Planetary Sciences, 28, 211-280.

Yin, A. and Taylor, M.H. (2011) Mechanics of V-shaped conjugate

strike-slip faults and the corresponding continuum mode of continental deformation. GSA Bulletin, 123, 1798-1821.

Zeng, R., He, C. and Kan, Y. (1961) The refracted waves and multiple waves in Chai-Da-Mu basin by low frequency seismic refraction work. Chinese Journal of Geophysics, 10(1), 39-53.

Zeng, R.-S. and Sun, W.-G. (1993) Seismicity and focal mechanism in Tibetan Plateau and its implications to lithospheric flow. Acta Seismologica Sinica, 6, 261-287.

Zhan, Z. and Kanamori, H. (2016) Recurring large deep earthquakes in Hindu Kush driven by a sinking slab. Geophysical Research Letters, 43, 7433-7441.

Zhang, J., Green, H.W., Bozhilov, K. and Jin, Z. (2004a) Faulting induced by precipitation of water at grain boundaries in hot subducting oceanic crust. Nature, 428, 633-636.

Zhang, P.-Z., Shen, Z., Wang, M., Gan, W.M., et al. (2004b) Continuous deformation of the Tibetan Plateau from global positioning system data. Geology, 32, 809-812.

Zhang, Z., Deng, Y., Teng, J., Wang, C., et al. (2011) An overview of the crustal structure of the Tibetan plateau after 35 years of deep seismic soundings. Journal of Asian Earth Sciences, 40, 977-989.

Zhang, Z., Deng, Y., Chen, L., Wu, J., et al. (2013) Seismic structure and rheology of the crust under mainland China. Gondwana Research, 23, 1455-1483.

Zhang, Z., Wang, Y., Houseman, G.A., Xu, T., et al. (2014) The Moho beneath western Tibet: Shear zones and eclogitization in the lower crust. Earth and Planetary Science Letters, 408, 370-377.

Zhao, J., Yuan, X., Liu, H., Kumar, P., et al. (2010) The boundary between the Indian and Asian tectonic plates below Tibet. Proceedings of the National Academy of Sciences, 107, 11229-11233.

Zhao, W., Nelson, K.D., Che, J., Quo, J., et al. (1993) Deep seismic reflection evidence for continental underthrusting beneath southern Tibet. Nature, 366, 557-559.

Zhao, Z., Niu, Y., Christensen, N.I., Zhou, W., et al. (2011) Delamination and ultra-deep subduction of continental crust: constraints from elastic wave velocity and density measurement in ultrahigh-pressure metamorphic rocks. Journal of Metamorphic Geology, 29, 781-801.

Zhou, B., Liang, X., Lin, G., Tian, X., et al. (2019) Upper crustal weak zone in Central Tibet: An implication from three-dimensional seismic velocity and attenuation tomography results. Journal of Geophysical Research: Solid Earth, 124, 4654-4672.

Zhou, H.-W. and Murphy, M.A. (2005) Tomographic evidence for wholesale underthrusting of India beneath the entire Tibetan plateau. Journal of Asian Earth Sciences, 25, 445-457.

Zhu, L. and Helmberger, D.V. (1996) Intermediate depth earthquakes beneath the India-Tibet Collision Zone. Geophysical Research Letters, 23, 435-438.

Manuscript received September 27, 2019
Manuscript accepted January 26, 2020
Published online March 27, 2020
Manuscript handled by Jun-ichi Ando Guest Editor